

Formation processes of tafoni on pyroclastic rock surfaces with hydrothermal alteration on the Isotake coast, Shimane, Japan

Tetsuya Kogure^{a,b,*}, Ryuya Sueyoshi^c, Hiroto Ohira^a, Yoshikazu Sampei^a, Ki-Cheol Shin^d, Yutaka Abe^e

^a Institute of Environmental Systems Science, Shimane University, 1060 Nishikawatsu-cho, Matsue, Shimane 690-8504, Japan

^b Center for Natural Disaster Reduction Research and Education, Shimane University, 1060 Nishikawatsu-cho, Matsue, Shimane 690-8504, Japan

^c Graduate School of Education, Shimane University, 1060 Nishikawatsu-cho, Matsue, Shimane 690-8504, Japan

^d Research Institute for Humanity and Nature, 457-4 Motoyama, Kamigamo, Kita-ku, Kyoto 603-8047, Japan

^e Natural Environment Conservation Centre, Nanasawa, Atsugi, Kanagawa 243-0121, Japan

ARTICLE INFO

Article history:

Received 31 March 2021

Received in revised form 15 November 2021

Accepted 19 November 2021

Available online 27 November 2021

Keywords:

Tafoni

Salt weathering

Hydrothermal alteration

Rockfall

ABSTRACT

Cliffs along the Isotake coast, Shimane, Japan, have two types of distinctive surfaces with different colours, with tafoni and without tafoni, even though they consist of the same pyroclastic rock. Rockfalls, which result in severe accidents, occur only on the surface without tafoni. Geochemical analyses of the cliff materials and the Schmidt hammer rebound test were conducted to elucidate the process of salt weathering in the formation of tafoni. The strontium stable isotope ratio ($^{87}\text{Sr}/^{86}\text{Sr}$) of the calcite (i.e., 0.706298) found on the backwall of tafoni indicated that the calcium in this calcite is derived from cliff materials, although the cliff receives seawater through splashing. Carbon, hydrogen, nitrogen and sulfur elemental analyses and X-ray diffraction pattern measurements revealed that clinoptilolite formed by hydrothermal alteration was more abundant in the cliff surfaces with tafoni than in those without tafoni, indicating a high abundance of calcium available for incorporation into calcite. The hardness of the cliff materials increases as the clinoptilolite content increases in any surface type. Consequently, tafoni preferentially form on surfaces with abundant clinoptilolite produced by hydrothermal alteration, although the surfaces have also been strengthened by hydrothermal alteration. Our results imply that the presence of tafoni indicates an overall lower risk of rockfalls.

© 2021 The Author(s). Published by Elsevier B.V. This is an open access article under the CC BY license (<http://creativecommons.org/licenses/by/4.0/>).

1. Introduction

A rockfall accident that caused a fatality occurred approximately 60 years ago at a pyroclastic rock cliff on the Isotake coast of Shimane, Japan. Rockfalls have occurred on cliff surfaces without tafoni (singular, tafone) even in recent years but have apparently not occurred on those with tafoni. Kogure et al. (2019) conducted the Schmidt hammer rebound test (SH test) on a tafone surface with a height and width of more than 10 m and a cliff surface without tafoni. This SH test found that the rebound value (R-value) of the tafone surface was significantly higher than that of the cliff surface without tafoni. The results are contrary to previous studies: the outer rock surfaces have a greater hardness than the rock interior (Conca and Rossman, 1982, 1985) or tafone backwalls, i.e., case hardening (Mottershead and Pye, 1994; Turkington, 1998; Goudie et al., 2002; Viles and Goudie, 2004); the differences may not be statistically significant (e.g., Mellor et al., 1997;

Matsukura and Tanaka, 2000; McBride and Picard, 2000; Mustoe, 2010; Roqué et al., 2013). Therefore, the tafone on the Isotake coast is unique in terms of its greater hardness than the outer rock surfaces. Further investigation will provide new insights into the tafoni formation process because, to the best of the authors' knowledge, no papers have investigated and discussed the formation process of such tafoni.

On the Isotake coast, Kogure et al. (2019) reported that calcite precipitates only on the backwall of tafoni, while it is absent on the cliff surfaces without tafoni. This situation implies that the tafoni formation process is associated with the salt weathering and that salt distribution characterizes the shape and stability of the cliff surfaces on the Isotake coast. Salt distribution is controlled by the distribution of moisture content (e.g., Huinink et al., 2004; Martinho et al., 2012; Schnepfleitner et al., 2016). Matsukura and Tanaka (2000) showed that tafoni caused by salt weathering arise on granite surfaces with higher moisture contents. The salt distribution is also affected by the distribution of specific minerals. For example, the concentration of clay minerals is positively correlated with the number of tafoni per surface area (Sancho and Benito, 1990). Considering that plenty of clay minerals, such as zeolite groups, are present in the rocks around the Isotake coast (Misumi and Ohira, 2006), the coastal cliffs are also likely to have clay minerals.

* Corresponding author at: Institute of Environmental Systems Science, Shimane University, 1060 Nishikawatsu-cho, Matsue, Shimane 690-8504, Japan.
E-mail address: kogure@riko.shimane-u.ac.jp (T. Kogure).

Since the clay minerals are always hydrates, the amount of clay minerals in a rock is evaluated by the measurement of hydrogen content in them. This is achieved by carbon, hydrogen, nitrogen and sulfur (CHNS) elemental analysis (Analytical Methods Committee, 2006): a higher hydrogen content indicates a larger amount of clay minerals in the rocks if the rocks originally have the same chemical composition. These techniques are valid if the tafoni are actually formed by the precipitation of calcite originating from chemical elements inherent to the cliff materials on the Isotake coast. On the other hand, calcium (Ca) used for the precipitation of calcite can be provided by seawater because the large tafone is located on the seaward part of the cliff surface (Kogure, 2019). Therefore, the origin of Ca should be identified to reveal the tafoni formation process although very few literatures reported calcite as a salt weathering mineral (e.g. Rothrock, 1925; Young, 1964).

This paper aims to discuss the factors and processes for the formation of tafoni on pyroclastic rock surfaces along the Isotake coast, where Kogure et al. (2019) evaluated the R-values and identified the precipitation of calcite on a single cliff. In this study, four sites were selected for investigation, from which rock and salt samples were collected in addition to the SH test and moisture measurements. The samples were used for CHNS elemental analysis to investigate the spatial distribution of hydrogen content and for X-ray diffraction (XRD) analysis to determine the types of minerals included in the rocks and salts. The strontium (Sr) stable isotope ratio ($^{87}\text{Sr}/^{86}\text{Sr}$) was also measured to identify the origin of Ca because Sr works as a trace element of Ca.

2. Study area

2.1. Environmental settings

The Isotake coast runs ENE–WSW and faces the Sea of Japan to the north on the coast of Ohda City, Shimane, Japan (Fig. 1a). Sandy beaches and coastal cliffs with heights exceeding 30 m develop along the coast

(Fig. 1b, c). Ohda City is located in a humid subtropical area, with an annual mean temperature and annual precipitation of 15.1 °C and 1738.4 mm, respectively (Japan Meteorological Agency). Fig. 2 shows climate data in Ohda city between 1981 and 2010. Although the monthly mean minimum temperature was above 0 °C (Fig. 2a), the nighttime low temperature dropped below 0 °C during nights of dozens of days each year (Fig. 2b). The geology of this area consists mainly of the Miocene Kuri Formation (Kano et al., 1998). The cliffs featuring the Kuri Formation are composed of rhyolitic pyroclastic rocks. These rocks were formed during the opening of the Sea of Japan, which occurred mainly during the interval 16.1–14.2 Ma (Otofuji et al., 1991). These rocks have subsequently been hydrothermally altered and subjected to low-grade metamorphism, resulting in extensive zeolite formation (Misumi and Ohira, 2006).

Cliffs along the Isotake coast are approximately 30 m in height, and the top surface is covered by vegetation (Fig. 3). Some of the cliffs have tafoni on their vertical surfaces, with maximum heights and widths exceeding 10 m and depths of several metres. No wave-cut notches can be seen on the cliff surfaces along the Isotake coast, whereas some caves are likely to have been formed by wave erosion (Fig. 3b, d).

2.2. Study cliffs

Four cliffs were selected for investigation (Figs. 1 and 3): Cliffs 1, 2, 3 and 4. Cliffs 1 and 2 have a tafone with a maximum width and length of 10 m and a depth of approximately 2 m, as shown in the enlarged photo in Fig. 3a and b, respectively. Cliff 3, which was investigated in Kogure et al. (2019), has the largest tafoni in the study area with the most distinctive surface: the vertical profile along Line A in Fig. 4a shows a large tafone, whereas the profile along Line B shows no tafoni (Fig. 4b). Cliff 4 is located in the eastern part of the study area, where the rock face is slightly different from other areas. Cliff 4 also has a cavernous structure; however, this appears to be a cave than a tafone. Therefore, we selected this cliff as an environmental reference for the study cliffs with tafoni.

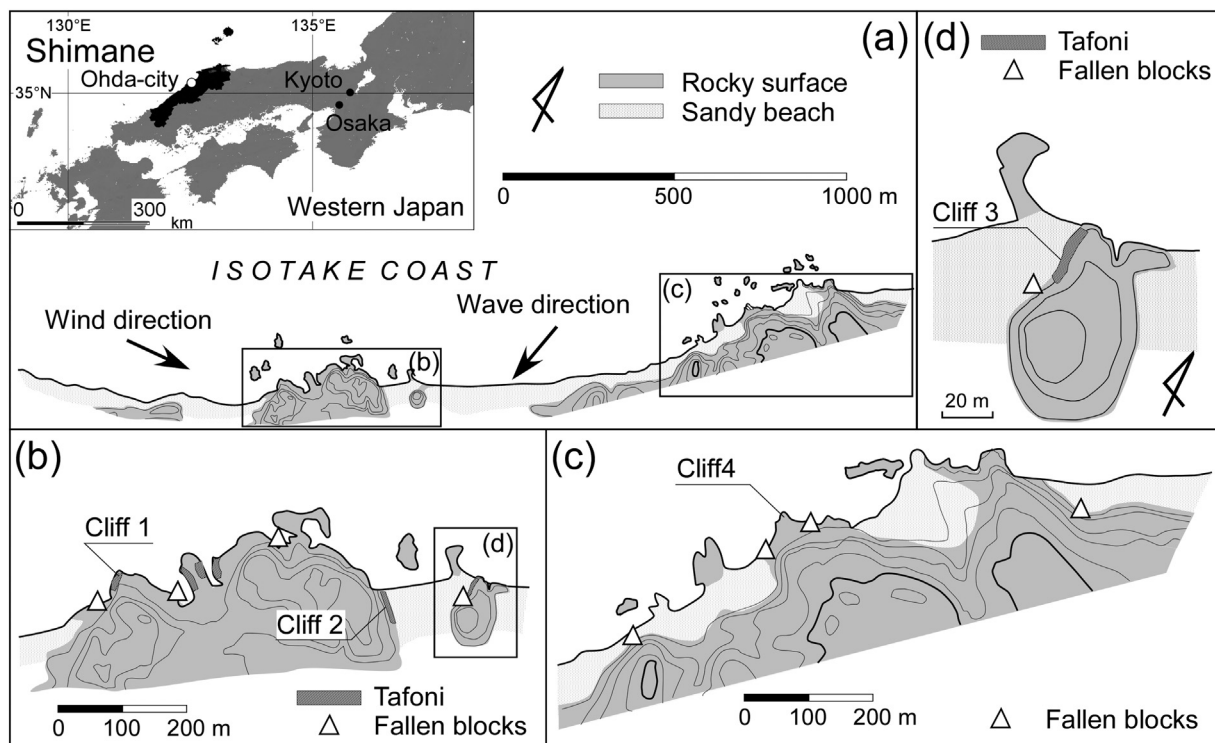


Fig. 1. Map of the cliffs along the Isotake coast: (a) map of the entire coast, (b) and (c) close-up maps of a part of the coast shown in Fig. 1a and (d) close-up map of the study site shown in Fig. 1b. The elevation shown via the bold contour line is 50 m above sea level, and the interval between contour lines is 10 m.

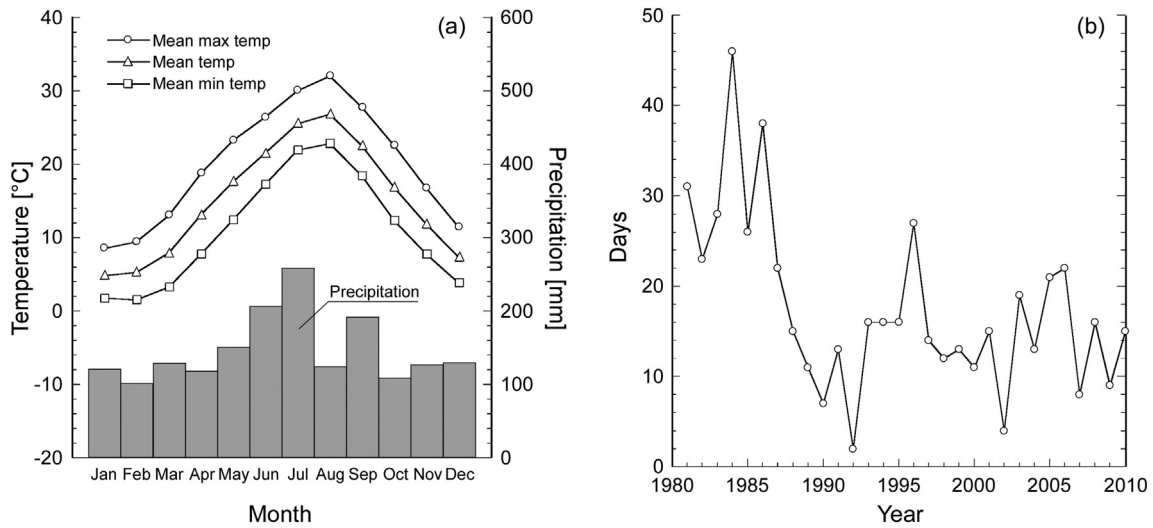


Fig. 2. Climate data from 1981 to 2010 in Ohda city derived from a weather station of the Japan Meteorological Agency located 5 km away from the study cliff: (a) changes in the monthly mean temperature and precipitation and (b) number of days for which the temperature dropped below 0 °C during night.

Some holes are found on part of the cliff surfaces surrounding the upper part of the tafoni (e.g., enlarged part in Fig. 4a). These holes have different sizes and shapes, and some of them seem to have coalesced to form a larger tafone. The cliff surface surrounding the large tafone in Fig. 4a has large hollows just beneath it (Fig. 4c, d). Therefore, the surfaces appear to be a thin crust with some holes connecting to the large hollows. This may be a sign of the tafoni growing upward that results in the enlargement of the tafoni.

The surfaces of cliffs with tafoni and surfaces without tafoni differ most noticeably in terms of the colour of these surfaces despite having the same geology on a microscopic level. The surfaces of cliff with tafoni are yellow-red with a middle value and various chroma in the Munsell soil colour charts (e.g., 10YR/5/2 for Fig. 5a and 10YR/6/6 for Fig. 5b), while the cliff surfaces without tafoni have higher values and lower chroma (e.g., 7.5YR/6/1 or 7.5YR/7/1 for Fig. 5c). The petrological characteristics of the rocks from both surfaces were investigated by thin

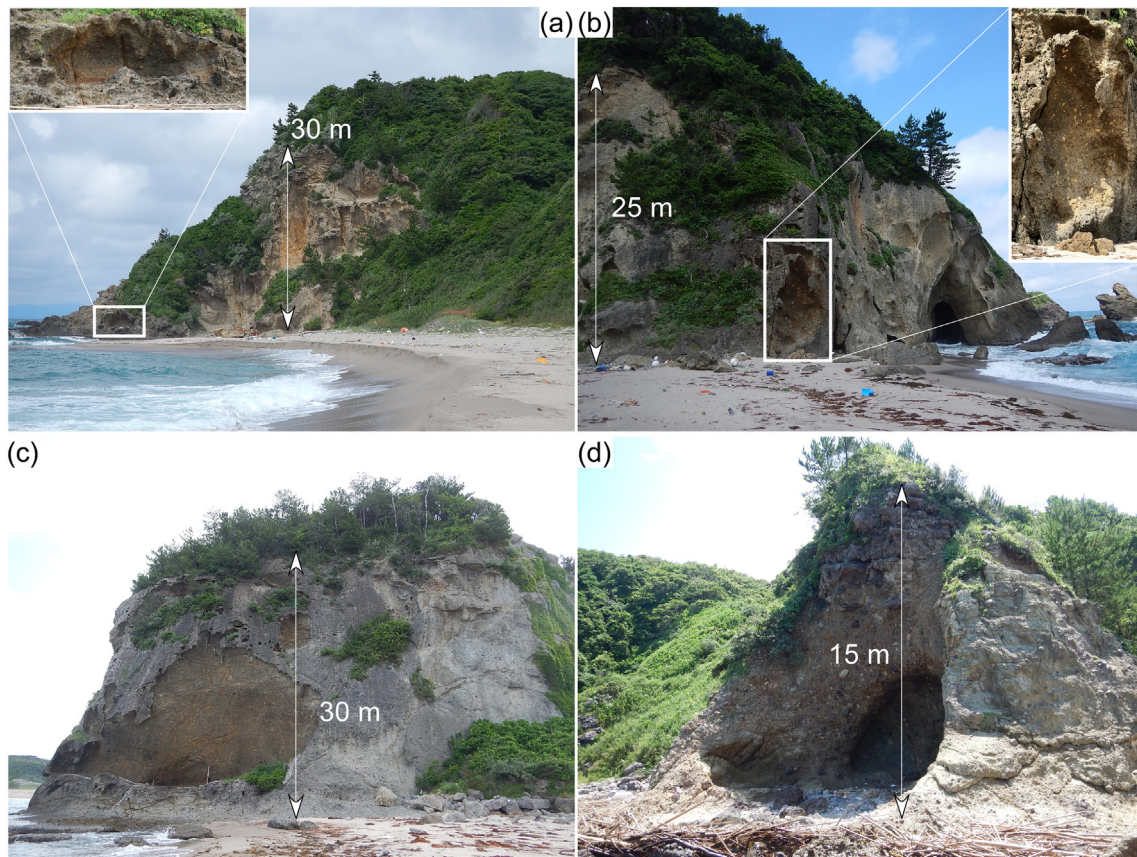


Fig. 3. Photos of the study cliffs: (a) Cliff 1, (b) Cliff 2, (c) Cliff 3 and (d) Cliff 4. The close-up photographs in Fig. 3a and b show the studied tafone in Cliffs 1 and 2, respectively. Cliff 3 is the same cliff as investigated in Kogure et al. (2019). This figure is available in colour online.

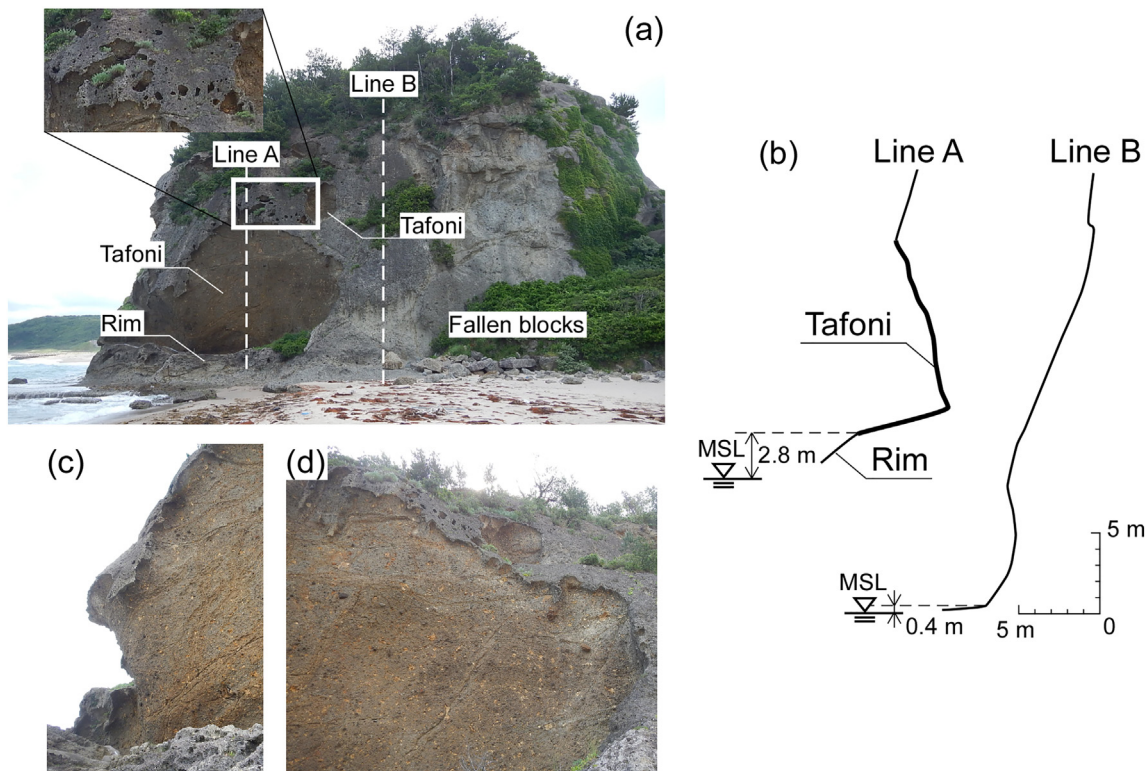


Fig. 4. Cliff 3 (modified after Kogure et al. (2019)): (a) vertical surfaces with tafoni on the seaward part and rockfalls on the inland part, (b) vertical profiles along Lines A and B in Fig. 4a, (c) a seaward part of the cliff surface surrounding the largest tafone and (d) inland part. The picture was taken from the west. This figure is available in colour online.

section analysis (Kogure, 2019). The photomicrographs of the pyroclastic rocks from the surfaces show that rocks from both surfaces have the same mineral composition, although the abundances and sizes of the grains differ (possibly caused by the heterogeneity in sediment structure). Therefore, the rock types of the surfaces are the same even though the colours of the surfaces differ.

Blocks with a maximum length of one to three metres accumulate at the base of Cliff 3 (Fig. 4a). Striations, which are seen on the cliff surface without tafoni and are just above the blocks, indicate that they are scars of the detachment of the blocks from the surface. However, the cliffs with tafoni have no accumulation of blocks at their base and no scars on their surface (Fig. 4a). This situation suggests that most of the rockfalls may occurred on the cliff surface without tafoni. The cliffs with rockfalls have no particular precipitates on their surfaces. Cliffs 1 and 2 have no surfaces that could become a potential source for rockfalls found at Cliff 3, although a few blocks exist at the base of each cliff (Fig. 3a, b).

2.3. Precipitates on the surface of tafoni

Yellow-red (10YR/6–8/8) precipitates on the surface of the tafoni suggest that they are responsible for the yellow-red colour of the surface (Fig. 5d). In contrast, almost no precipitates are seen on the cliff surface without tafoni (Fig. 5c).

Most precipitates appear on the backwall of tafoni with a flat face (Fig. 5e) or with one moderately expanded face (Fig. 5f). Furthermore, precipitates that have a flower-like structure (Fig. 5g) can be found at a relatively lower frequency. The flower-like precipitates have already been identified to be calcite through XRD analysis (Fig. 5h, Kogure, 2019). The maximum length of the expanded calcite is approximately 10 cm. Flower-like structures are easily broken by the impact of a rock hammer.

The precipitates on the backwall of tafoni appear to induce the detachment of small fragments of the pyroclastic rock and gravel from the surface during their growths, as evidenced by the accumulation of

small fragments and gravel at the foot of the tafoni. We confirm that some precipitates have grown on the cliff surfaces from which gravel has detached based on the observation of detachment scars in moulded shapes (Fig. 5a, b, g).

2.4. Rock hardness

To investigate the mechanical characteristics of the cliff rock, Kogure et al. (2019) applied the SH test to the cliff surface with and without tafoni (Cliff 3 in the present study). This is because the R-value of the SH test is closely related to the uniaxial compressive strength (UCS) (e.g., Aydin and Basu, 2005), which is used to evaluate the mechanical characteristics of rocks. Kogure et al. (2019) adopted the continuous (repeated) impact method proposed by Matsukura and Aoki (2004), who explained that repeated impacts at the same point without any release of the hammer from the rock surface generate an understanding of the degree of weathering of the surface and make it possible to assess the hardness of the intact rock. The R-value increases as the number of repeated impacts increases because weathered surfaces that are loose become firm due to compaction of the grains.

In Kogure et al. (2019), the results of the SH test clearly distinguished that the surface with tafoni has higher R-values than the surface without tafoni (Table 1). The maximum and minimum R-values in 20 impact repetitions, R_{\max} and R_{\min} , reflect the strength of the inner body and surface of the cliff, respectively (Table 1, Kogure, 2019). The differences in R_{\max} , R_{\min} and standard deviation values between the surfaces suggest that they have different physical and mechanical properties despite composed of same rock type.

3. Methods

3.1. Samples for geochemical analyses

Fig. 6 shows the sampling points. Table 2 presents the list of samples. Rock samples were selected from the matrix of the surface of tafoni or

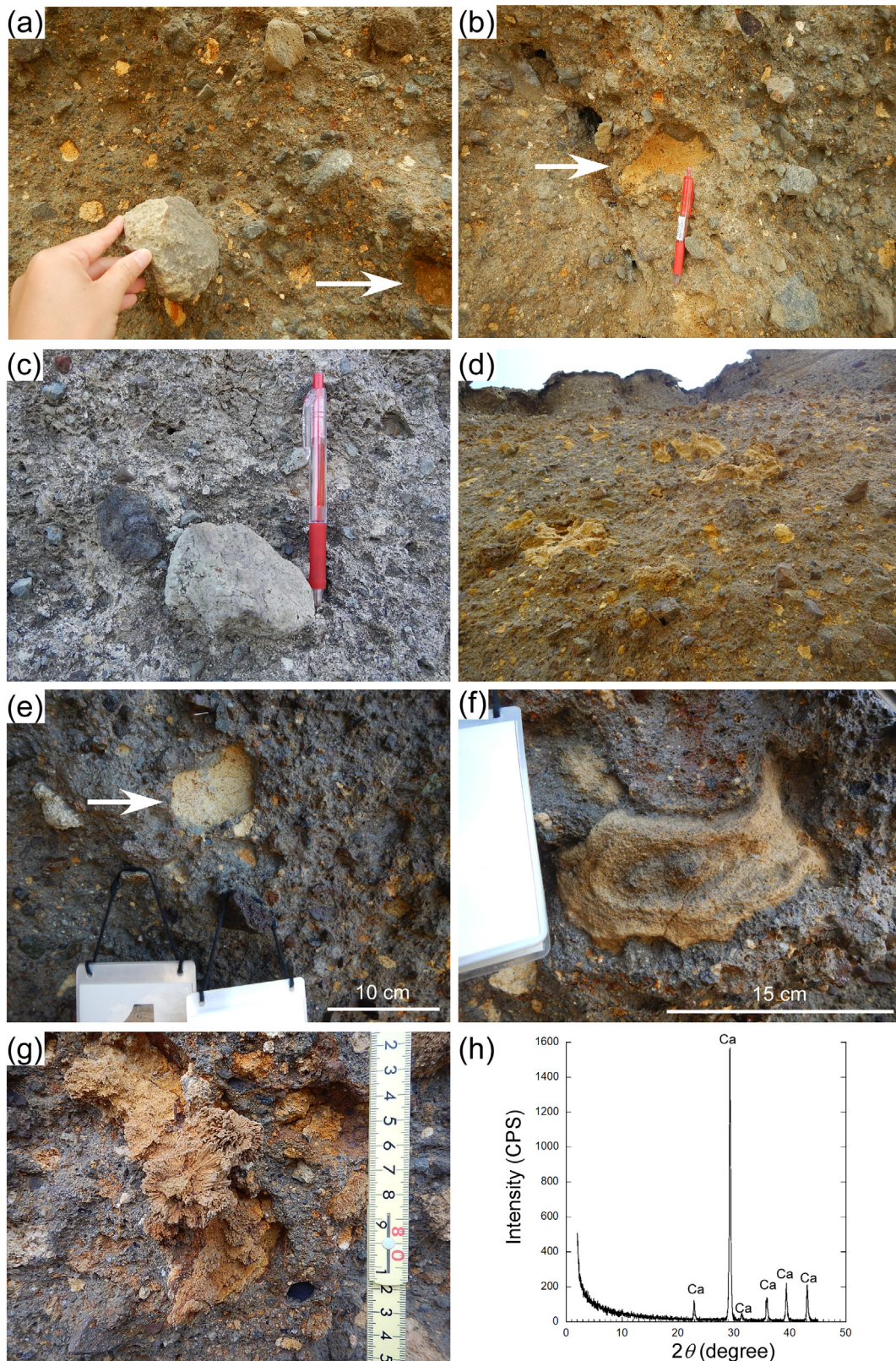


Fig. 5. Close-up photos of cliff surfaces: (a) backwall of tafoni in Cliff 3, (b) backwall of tafoni with the detachment scar of gravel in Cliff 3, (c) without tafoni in Cliff 3, (d) projection of precipitates and gravel from the surface of tafoni in Cliff 3, (e) a precipitate without expansion (No. 1-S4), (f) a precipitate with moderate expansion (No. 1-S5), (g) a flower-like salt (No. 3-S7) and (h) XRD pattern of the salt in Fig. 5g (Kogure, 2019). The abbreviation “Ca” denotes calcite in Fig. 5h. The arrows in Fig. 5a, b and e show examples of the detachment scars of gravel or boulder. Fig. 5c was taken looking upward along the surface of the largest tafone in Cliff 3. This figure is available in colour online.

cave (Cliff 1–4), cliffs outside tafoni or cave (Cliff 1–4), bottom rim of tafoni (Cliff 1–3) and transition zone from the backwall of tafoni to cliff surface outside tafoni (Cliff 3). Precipitate samples were collected

from the backwall of tafoni or cave with different precipitate shapes: a precipitate without notable expansion (Fig. 5e), a moderately expanded precipitate without a flower-like part (Fig. 5f) and a flower-like salt

Table 1
Summary of the results of the SH test by Kogure et al. (2019).

Surface type (Number of SH test)	Tafoni (26)		Cliff surface without tafoni (22)	
	R_{max}	R_{min}	R_{max}	R_{min}
Maximum	63	36	48	22
Mean	59.0	24.4	37.7	14.8
Minimum	54	13	28	12
Standard deviation	2.6	6.4	5.1	2.1

mentioned by Kogure et al. (2019) (Fig. 5g). Flower-like salt was found and collected only from Cliff 3.

Fig. 7 shows some of the collected samples. Many of the precipitates were powdered during sampling because they were unconsolidated. All of the samples were dried at 110 °C for more than 24 h before the preparation of each chemical measurement.

3.2. Strontium isotope measurements

Isotopic measurements are well known and used to determine the origin of chemical elements even in tafoni studies (e.g., McBride and Picard, 2000). On the Isotake coast, Ca ions need to be provided to the cliff surface for the precipitation of calcite. Igneous rocks can provide Ca because they are composed of various types of minerals with metallic or nonmetallic elements. Seawater might also have provided Ca to the surface through splashing. In addition to Ca, both igneous rocks and seawater contain Sr as a trace element. Strontium can be incorporated into calcite during its formation, and the mechanisms of Sr incorporation have been widely studied in biogenic (e.g., Lea et al., 1999) and inorganic (e.g., Tesoriero and Pankow, 1996; Wasylenki et al., 2005) calcite. Thus, Sr is present in Ca-bearing minerals such as plagioclase and amphibole, and is a useful tool to determine the origin of Ca. The measurement of the $^{87}\text{Sr}/^{86}\text{Sr}$ ratio in Ca-bearing minerals allows us to identify the source of Sr, which is considered to be the same as that of Ca. The $^{87}\text{Sr}/^{86}\text{Sr}$ ratio measurements in water and Holocene marine carbonates show that the values of the present-day seawater are 0.709241 ± 0.000032 and 0.709211 ± 0.000037 , respectively (Elderfield, 1986). The $^{87}\text{Sr}/^{86}\text{Sr}$ isotopic compositions of the Miocene volcanic rocks on the Shimane Peninsula is in the range of 0.70417–0.70652 (Iizumi et al., 1999). Water migrating through specific flow paths, including high permeability/porosity zones or successions of structural discontinuities in rocks, react with the rocks, resulting in the equilibrium in $^{87}\text{Sr}/^{86}\text{Sr}$ ratios between the water and rocks. Consequently, the $^{87}\text{Sr}/^{86}\text{Sr}$ ratio in calcite should be almost equal to that in seawater if Ca is provided by seawater or to that in cliff material if Ca is contributed by freshwater permeating the cliffs.

Measurements were conducted for almost all the samples (Table 2). The samples of the rocks and precipitates (Fig. 7) were broken into smaller portions of volume of ca. 1 cm³. We considered that the ca. 1 cm³ portions are large enough to represent the homogeneity of the rocks and precipitates. These portions were powdered, and ca. 0.5 g of each sample was used for the analysis. Leachate obtained from the reaction between 5% ammonium acetate and powdered samples was used for the measurements. The Sr in the samples was separated and purified by standard ion exchange chromatography before the measurements. The isotopic ratio was determined by multicollector double-focusing inductively coupled plasma mass spectrometry (ICP-MS; Neptune Plus, Thermo Fisher Scientific, Bremen, Germany) at the Research Institute for Humanity and Nature. The values and processes used to calculate the $^{87}\text{Sr}/^{86}\text{Sr}$ ratio with high accuracy were as follows. The $^{87}\text{Sr}/^{86}\text{Sr}$ ratios were internally normalized to an $^{86}\text{Sr}/^{88}\text{Sr}$ ratio of 0.1194. Replicate analyses of the NIST SRM 987 standard during this study yielded an $^{87}\text{Sr}/^{86}\text{Sr}$ ratio of 0.710302 ± 0.000014 (mean \pm SD, $n = 4$). The standard deviation of the $^{87}\text{Sr}/^{86}\text{Sr}$ ratio of all the samples was lower than

0.000010. All the measurements were normalized to the $^{87}\text{Sr}/^{86}\text{Sr}$ ratio of 0.71025 recommended by Faure and Mensing (2004).

3.3. Measurement of X-ray diffraction patterns

The XRD patterns of 20 samples were measured to identify the minerals present in the precipitates and the cliff surfaces (Table 2). Considering that the zeolite series usually occurs along miscellaneous joints and cavities in rocks in active thermal areas (e.g., Coombs et al., 1959), the XRD patterns can vary with the sampling location. The patterns were recorded by a Rigaku diffractometer, SmartLab at Shimane Institute for Industrial Technology for samples No. 3-S3 and —S4. Rint 2000 at Shimane University was used for the analysis of other samples. The settings for SmartLab and Rint 2000 were CuK α at 40 kV and 40 mA and CuK α at 30 kV and 20 mA, respectively. The analysis was performed between 3° and 50° at 2 θ , steps of 0.02 and a scan speed of 10° per minute for SmartLab and between 2° and 50° at 2 θ , steps of 0.02 and a scan speed of 2° per minute for Rint 2000.

3.4. CHNS elemental analysis

According to the Analytical Methods Committee (2006), the principle of this analysis can be simply summarized as follows. Simultaneous CHNS analysis requires high-temperature combustion (ca. 1000 °C) in an oxygen-rich environment. In the combustion process, carbon is converted to carbon dioxide, hydrogen to water, nitrogen to nitrogen gas/oxides of nitrogen and sulfur to sulfur dioxide/trioxide. The gases are then passed through the absorbent traps to leave carbon dioxide, water, nitrogen and sulfur dioxide. Finally, the elements are successfully quantified.

The CHNS analysis was conducted for 46 samples (Table 2) using a CHNS elemental analyser (FIONS EA1108) at Shimane University. As described in 3.2, the samples of the rocks and precipitates (Fig. 7) were broken into smaller portions, each with a volume of ca. 1 cm³. Then, these portions were powdered. After being dried in an oven, 10 mg of each sample was placed in the analyser. BBOT (the abbreviation of 2,5-Bis-(5-tert-butyl-benzo-oxazol-2-yl)-thiophen) was used as a standard, and a standard regression line based on 5 points was employed for the quantitative analysis. Errors (coefficient of variation) inherent to this analysis were within $\pm 3\%$ for total organic carbon (TOC), total hydrogen (TH) and total nitrogen (TN), and $\pm 4\%$ for total sulfur (TS) (Sampei et al., 1997).

3.5. Measurement of the moisture content

The moisture content, w , of rock surfaces can be measured by moisture metres (e.g., Matsukura and Takahashi, 1999; Eklund et al., 2013). We used a portable infrared optical moisture meter (JE100 manufactured by Japanese Tobacco Engineering Co.) introduced by Matsukura and Takahashi (1999). This device measures the absorbance intensity of the near-infrared rays reflected from the surface, X , with a measurement error within $\pm 2.5\%$. Calibration was conducted prior to the measurements following the instructions suggested by Matsukura and Takahashi (1999). We used amorphous pieces of rocks with a volume of ca. 100 cm³ obtained from the backwall of tafoni at Cliff 3 for calibration, and formulated an equation to calculate the value of w (%):

$$w = 17.5X. \quad (1)$$

The X -values derived from the measurements were converted to the moisture content of the backwall of tafoni with Eq. (1).

We investigated hourly changes in moisture content with different purposes. One was the measurement on the backwall of tafoni at Cliff 3 to understand the vertical distribution of moisture content on it. Measurement points were aligned on lines parallel to Line A with vertical and horizontal intervals of 1 m and 2 m, respectively (Lines A, C, D

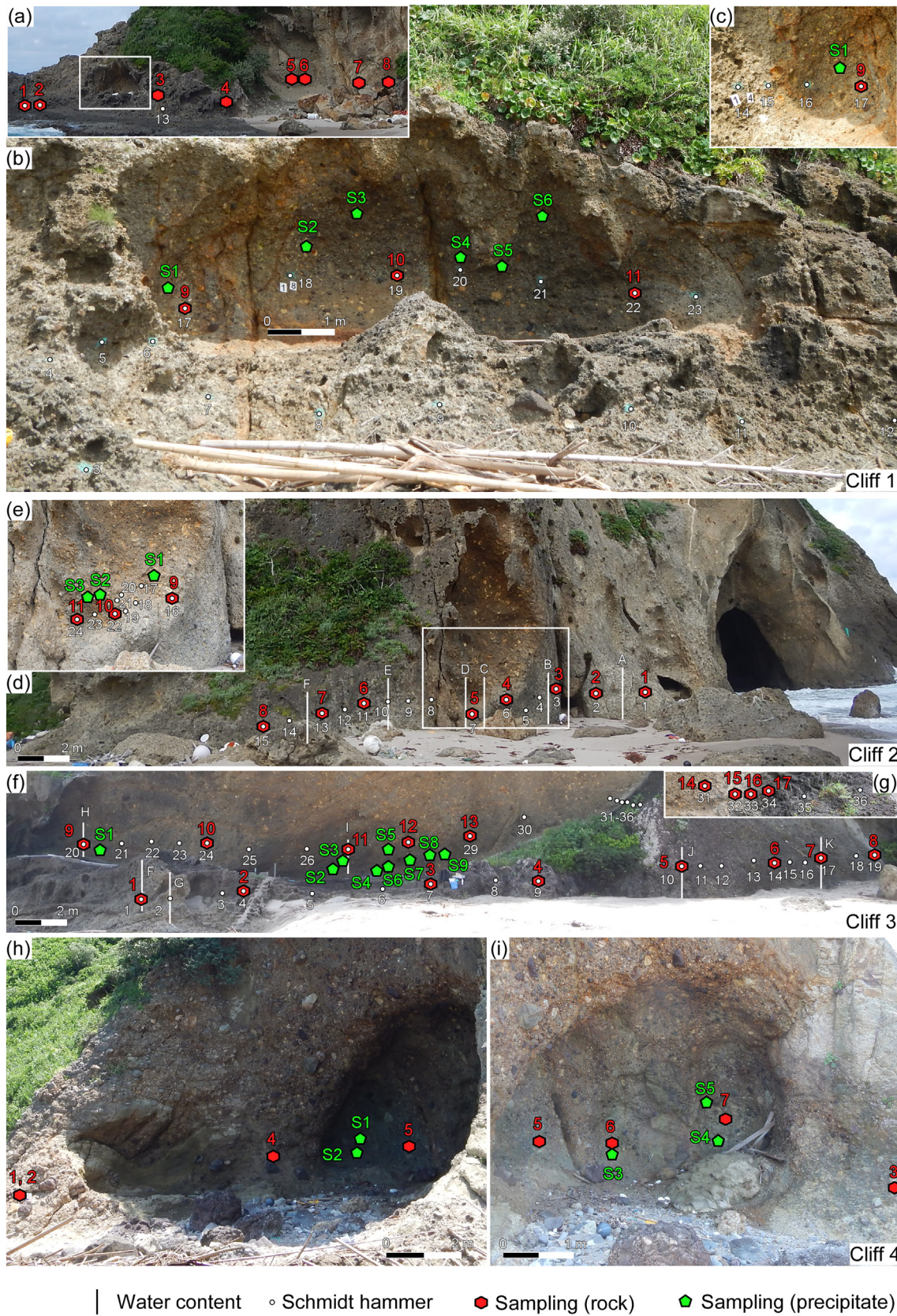


Fig. 6. Points for measurements and sampling sites: (a) Cliff 1, (b) studied tafone in Cliff 1 shown in the box in Fig. 6a, (c) a view of a sidewall on the left side of the tafone in Fig. 6b, (d) Cliff 2, (e) enlarged photo of the tafone in the box in Fig. 6e, (f) Cliff 3, (g) transition zone from the backwall of tafoni to the cliff surface without tafoni, (h) Cliff 4 and (i) inside the cave in Cliff 4. This figure is available in colour online.

Table 2
Rock and precipitate samples for geochemical analyses.

Sample No.	Sample type	Surface	⁸⁷ Sr/ ⁸⁶ Sr	Error	⁸⁷ Sr/ ⁸⁶ Sr (bulk)	Error	CHNS (wt%)				XRD pattern
							TN	TOC	TH	TS	
Cliff 1											
1-1	Rock	Without tafoni	0.708241	0.000014			0.010	0.868	0.012	0.000	
1-2	ditto	ditto	n/a	n/a			0.011	0.189	1.091	0.016	Fig. 10
1-3	ditto	ditto	0.708735	0.000007			0.016	1.718	1.303	0.001	
1-4	ditto	ditto	0.707016	0.000009			n/a	n/a	n/a	n/a	
1-5	ditto	ditto	0.705195	0.000007			n/a	n/a	n/a	n/a	
1-6	ditto	ditto	0.705205	0.000006			n/a	n/a	n/a	n/a	
1-7	ditto	ditto	0.705187	0.000008			n/a	n/a	n/a	n/a	
1-8	ditto	ditto	0.705194	0.000007			n/a	n/a	n/a	n/a	
1-9	ditto	Tafoni	0.705221	0.000009			0.005	1.196	1.484	0.380	
1-10	ditto	ditto	0.705283	0.000009			0.004	0.308	0.865	0.065	Fig. 10
1-11	ditto	ditto	0.705597	0.000011			0.002	0.307	0.696	0.095	
1-S1	Precipitate	ditto	0.705231	0.000009			0.004	0.222	2.563	0.219	
1-S2	ditto	ditto	0.705238	0.000007			n/a	n/a	n/a	n/a	
1-S3	ditto	ditto	0.705227	0.000007			0.006	0.611	2.177	0.038	
1-S4	ditto	ditto	0.705231	0.000008			0.007	0.283	1.477	0.173	Fig. 10
1-S5	ditto	ditto	0.705227	0.000008			0.006	3.108	2.257	0.037	Fig. 10
1-S6	ditto	ditto	0.705244	0.000009			n/a	n/a	n/a	n/a	
Cliff 2											
2-1	Rock	Without tafoni	0.707701	0.000003			n/a	n/a	n/a	n/a	
2-2	ditto	ditto	0.708546	0.000005			0.001	0.287	0.598	0.016	Fig. 10
2-3	ditto	ditto	0.706759	0.000004			0.002	0.097	0.759	0.048	
2-4	ditto	ditto	0.707400	0.000004			0.001	0.109	0.439	0.131	Fig. 10
2-5	ditto	ditto	0.707070	0.000005			0.001	0.212	0.668	0.047	
2-6	ditto	ditto	0.707587	0.000004			0.010	0.142	0.792	0.000	
2-7	ditto	ditto	0.708162	0.000004			n/a	n/a	n/a	n/a	
2-8	ditto	ditto	0.708589	0.000003			0.012	0.807	1.245	0.036	
2-9	ditto	Tafoni	0.705592	0.000003			0.002	0.114	0.688	0.269	
2-10	ditto	ditto	0.705721	0.000004			0.001	0.090	0.850	0.060	Fig. 10
2-11	ditto	ditto	0.705998	0.000004			0.002	0.082	0.762	0.049	
2-S1	Precipitate	ditto	0.705562	0.000003			0.004	0.003	2.358	0.209	Fig. 10
2-S2	ditto	ditto	0.705743	0.000004			0.006	0.003	2.811	0.433	
2-S3	ditto	ditto	0.705812	0.000004			0.004	0.000	1.922	0.063	Fig. 10
Cliff 3											
3-1	Rock	Bottom rim	0.708333	0.000003			0.003	0.410	0.582	0.011	
3-2	ditto	ditto	0.708845	0.000003			0.010	0.067	0.923	0.004	Fig. 10
3-3	ditto	ditto	0.708815	0.000014	0.708173	0.000008	0.036	0.273	1.716	0.020	Fig. 10
3-4	ditto	ditto	0.708551	0.000003			0.035	0.333	0.724	0.062	
3-5	ditto	Without tafoni	0.707044	0.000003			0.020	0.284	0.924	0.015	
3-6	ditto	ditto	0.705890	0.000004			0.005	0.158	0.698	0.069	
3-7	ditto	ditto	0.705845	0.000013	0.705247	0.000007	0.006	0.102	0.199	0.000	Fig. 10
3-8	ditto	ditto	0.705377	0.000003			0.000	0.508	0.491	0.189	
3-9	ditto	Tafoni	0.705330	0.000004			0.001	0.009	1.158	0.040	
3-10	ditto	ditto	0.705312	0.000004			0.005	0.091	0.895	0.121	
3-11	ditto	ditto	0.705372	0.000012	0.705330	0.000009	0.017	0.073	1.947	0.000	Fig. 10
3-12	ditto	ditto	0.705524	0.000014	0.705353	0.000006	n/a	n/a	n/a	n/a	
3-13	ditto	ditto	0.705671	0.000008	0.705422	0.000006	n/a	n/a	n/a	n/a	
3-14	ditto	ditto	0.705566	0.000003			0.002	0.055	0.135	0.037	
3-15	ditto	Transition zone	0.705660	0.000004			0.019	0.221	0.692	0.033	Fig. 10
3-16	ditto	ditto	0.705798	0.000004			0.016	0.261	0.661	0.042	Fig. 10
3-17	ditto	ditto	0.706110	0.000004			0.028	0.363	0.623	0.006	Fig. 10
3-S1	Precipitate	Tafoni	0.705662	0.000004			0.001	8.853	0.000	0.094	
3-S2	ditto	ditto	0.705425	0.000007			0.019	0.287	10.798	0.491	
3-S3	ditto	ditto	0.705435	0.000004			0.002	4.438	0.625	0.000	Fig. 10
3-S4	ditto	ditto	0.705420	0.000004			0.001	2.756	0.981	0.000	Fig. 10
3-S5	ditto	ditto	0.705702	0.000005			0.011	8.559	0.062	0.030	Fig. 10
3-S6	ditto	ditto	0.705343	0.000005			0.015	0.957	2.798	0.263	
3-S7	ditto	ditto	0.706298	0.000012			0.000	10.112	0.000	0.000	Fig. 5h
3-S8	ditto	ditto	0.705667	0.000011			0.000	4.725	1.052	0.000	
3-S9	ditto	ditto	0.705444	0.000011			0.000	0.000	2.284	0.000	Fig. 10
Cliff 4											
4-1	Rock	Without cave	0.706323	0.000010			n/a	n/a	n/a	n/a	
4-2	ditto	ditto	0.707954	0.000008			n/a	n/a	n/a	n/a	
4-3	ditto	ditto	0.706536	0.000007			n/a	n/a	n/a	n/a	
4-4	ditto	ditto	0.705726	0.000008			n/a	n/a	n/a	n/a	
4-5	ditto	Cave	0.705358	0.000008			n/a	n/a	n/a	n/a	
4-6	ditto	ditto	0.705393	0.000008			n/a	n/a	n/a	n/a	
4-7	ditto	ditto	0.705256	0.000009			n/a	n/a	n/a	n/a	
4-S1	Precipitate	ditto	0.705413	0.000008			n/a	n/a	n/a	n/a	
4-S2	ditto	ditto	0.705604	0.000010			n/a	n/a	n/a	n/a	
4-S3	ditto	ditto	0.705418	0.000008			n/a	n/a	n/a	n/a	

Table 2 (continued)

Sample No.	Sample type	Surface	$^{87}\text{Sr}/^{86}\text{Sr}$	Error	$^{87}\text{Sr}/^{86}\text{Sr}$ (bulk)	Error	CHNS (wt%)				XRD pattern
							TN	TOC	TH	TS	
4-S4	ditto	ditto	0.705313	0.000010			n/a	n/a	n/a	n/a	
4-S5	ditto	ditto	0.705268	0.000009			n/a	n/a	n/a	n/a	

and E in Fig. 8a). The lowest points correspond to the deepest part of the tafoni, which is equal to ca. 4.4 m above MSL. The vertical profile of each line is similar to that of Line A (Fig. 4b). The measurement was conducted from 10:30 to 15:30 on 20th October 2016.

The other measurement was on both the backwall of tafoni and the cliff surfaces without tafoni at Cliff 2 and Cliff 3 to understand the spatial distribution of moisture content around a cliff with tafoni. Measurements were conducted for Lines A – F on Cliff 2 (Fig. 6d) and Lines F – K on Cliff 3 (Fig. 6f), which are 2 m long, and measurement points were set on the vertical lines every meter. The bottom end of the lines was set on the vertical surface of the cliff or tafoni slightly above the intersection of the vertical surface and horizontal floor. The measurement was conducted from 10:00 to 15:00 for Cliff 3 and 12:00 to 15:00 for Cliff 2 on 26th November 2020. Detailed climate conditions are shown in Fig. 8b, c and d.

3.6. Schmidt hammer rebound test

The hammer used in this study was a GS-type for rocks, made by Sanyo Testing Machines Co., Japan, having an impact energy of 2.207 Nm. The SH test was conducted at Cliffs 1, 2 and 3 (Fig. 6) in the same manner as shown in Kogure et al. (2019): each test involved 20 impact repetitions. The impact points on Cliff 3 were not different from those by Kogure et al. (2019), whose tests were also conducted on the same cliff surface. Our tests included the impacts on the transition zone from the largest tafone surface to the cliff surface without tafoni in Cliff 3 (Fig. 6f, g).

4. Results

4.1. Strontium isotope ratio and origin of calcite in calcite

Table 2 lists the results of the measurements of $^{87}\text{Sr}/^{86}\text{Sr}$. The term “bulk” means that the volume of the samples was larger (but smaller than 1 cm^3) compared to the ordinary $^{87}\text{Sr}/^{86}\text{Sr}$ measurements and this is large enough to include some small clasts. The bulk samples were used to mitigate the effect of contamination on the ordinary measurements because the $^{87}\text{Sr}/^{86}\text{Sr}$ ratio of a smaller volume of matrix could be affected by the presence of specific minerals with extremely high or low values. In reality, the measurements of the small and large samples showed almost the same $^{87}\text{Sr}/^{86}\text{Sr}$ values, ensuring the validity of the measurements.

The results show that the $^{87}\text{Sr}/^{86}\text{Sr}$ ratios in the rocks and precipitates on the backwall of tafoni are 0.705221–0.705597 for Cliff 1, 0.705562–0.705998 for Cliff 2 and 0.705312–0.706298 for Cliff 3 (Tables 2 and 3). These values are in the ranges reported by Iizumi et al. (1999), indicating that the rhyolitic pyroclastic rocks of the study cliff have $^{87}\text{Sr}/^{86}\text{Sr}$ ratios that are typical of the Miocene volcanic rocks in the Shimane Peninsula and that the salts originated from rhyolitic rocks. The value, 0.706298, obtained from sample No. 3-S7 is slightly higher than that from the cliff matrix ratio values. Therefore, the limited influence of seawater on the precipitation of calcite cannot be ruled out. However, considering that the $^{87}\text{Sr}/^{86}\text{Sr}$ ratio in sample No. 3-S7 is significantly lower than that of seawater (approximately 0.7092 as mentioned above) and that the values of the salts are almost the same as those of the rocks (Table 2 and Fig. 9a), most of the Ca in the precipitated calcite appears to have originated from the pyroclastic rocks in the cliffs.

The values in the rocks from the surface without tafoni and bottom rim of the tafoni vary with location (Fig. 9a). They are higher on the

surfaces where much seawater available through splashing (e.g., No. 1–1 to 1–4 in Fig. 6a) than on the surfaces where less splashing occurs (e.g., No. 1–5 to 1–8 in Fig. 6a). Furthermore, the higher values are close to the present-day seawater value (Fig. 9a). A similar trend is also found in Cliff 4 (wave-cut cave): the rock surfaces outside the cave have higher $^{87}\text{Sr}/^{86}\text{Sr}$ ratios than those in rocks and precipitates on the cave surface (Tables 2 and 3). Therefore, the higher $^{87}\text{Sr}/^{86}\text{Sr}$ ratios indicate that the surfaces have been affected by seawater.

4.2. XRD patterns and distribution of precipitates

Fig. 10 shows the XRD patterns of the rocks and precipitates. The patterns reveal that almost all the samples contain clinoptilolite ((Na, K, Ca_{0.5})₆(Al₆Si₃₀O₇₂)·20H₂O). These variations are produced by cation substitution between Na, K and Ca. Therefore, clinoptilolite contains Ca as a chemical component and appears to be a possible source of the Ca involved in the precipitation of calcite. The composition of the remaining clinoptilolite changes to Ca-depleted clinoptilolite-Na or clinoptilolite-K. Clinoptilolite is a secondary mineral defined as a member of the zeolite mineral series (e.g., Coombs et al., 1997). The temperature conditions for the occurrence of the zeolite series vary from 200 °C to 300 °C, depending on the pressure. Yoshida (1979) noted that the zeolite minerals in the study area were formed by the intrusion of rhyolite occurring at the end of volcanism. Clinoptilolite must therefore have also been precipitated in the hydrothermal alteration stage following the volcanism. There is no active volcanism near the study area at the present time which implies that clinoptilolite must have formed a long time ago (ca. 16–14 Ma).

Halite (NaCl) is also observed in some samples from both rocks and precipitates. However, no halite was detected from the samples from Cliff 3 although the number of samples analysed were the largest among the studied cliffs. The lack of halite in Cliff 3 could be attributed to the lower susceptibility of direct waves to the Cliff 3 relative to Cliffs 1 and 2. Calcite was detected only from No. 3-S5 (Fig. 7), a flower-like salt reported by Kogure et al. (2019), which is not seen on the backwall of tafoni in Cliffs 1 and 2. The absence of calcite on the rocks other than precipitates supports that clinoptilolite is a source of Ca for the precipitation of calcite, and suggests that the detection of calcite can be achieved by the formation of matured calcite crystal. These results indicate that tafoni formation process differs between the cliffs: salt weathering results in the formation of tafoni is mainly caused by halite for Cliffs 1 and 2 and calcite for Cliff 3.

The XRD patterns of most of the rocks inside and outside of the tafoni are similar: quartz and plagioclase, which are the major components of rhyolite, are identified in addition to clinoptilolite. The XRD pattern of the cliff surface without tafoni in Cliff 3, No. 3–7 has also quartz and plagioclase. However, no particular peaks associated with clinoptilolite are observed in No. 3–7: the lack of the peak at approximately $2\theta = 10$ that is clearly identified in other rocks and precipitates. This result is consistent with our observation that there are fewer precipitates on the cliff surface without tafoni (Fig. 5c), implying that the clinoptilolite content of the rocks varies with location in the study cliffs.

4.3. CHNS elemental analysis

Tables 2 and 3 and Fig. 9b show the results of the CHNS analysis. The mean total hydrogen content (TH, wt%) in the backwall of tafoni (= 1.034) is approximately 2 times higher than averaged values in the

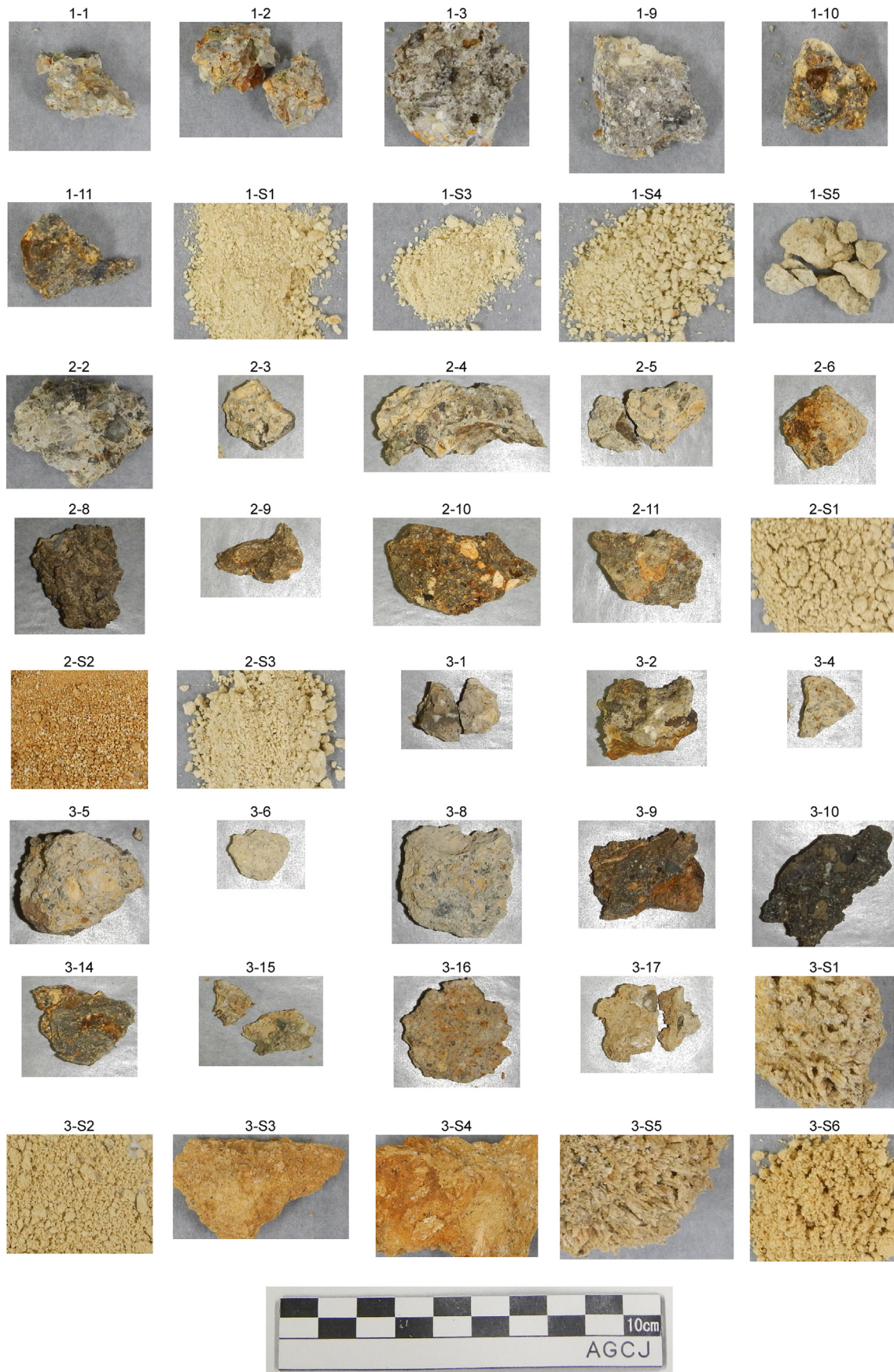


Fig. 7. Samples of rocks and precipitates used for geochemical analyses. This figure is available in colour online.

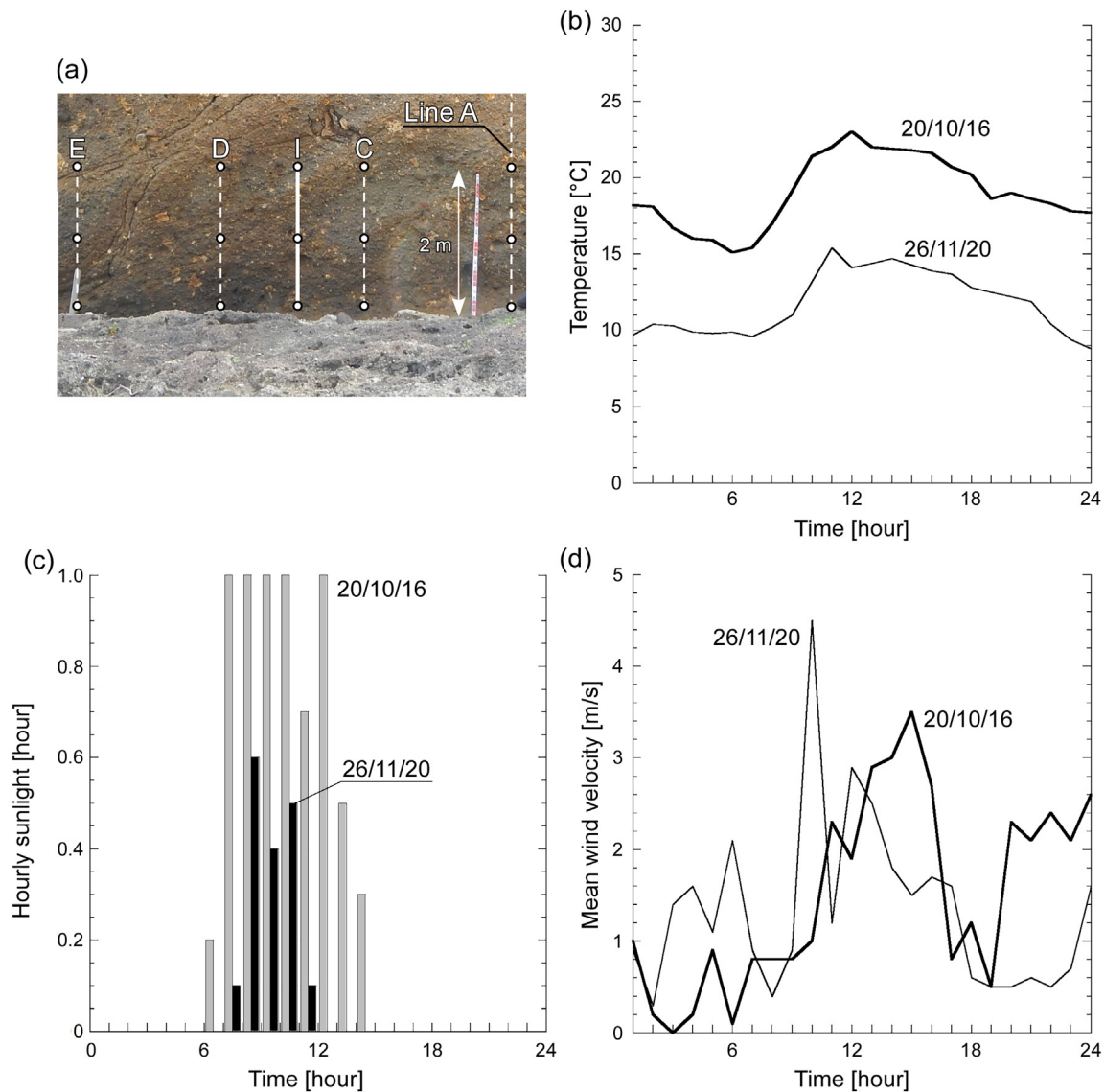


Fig. 8. Measurement of moisture content: (a) measurement points along Lines A, C, D and E, (b), (c) and (d) hourly changes in the temperature, sunlight and wind velocity, respectively, on 20th October 2016 and 26th November 2020. Line A corresponds to that in Fig. 4a and b. The climate conditions were measured at an inland weather station located 5 km away from the cliff. This figure is available in colour online.

cliff surface without tafoni (= 0.578) in Cliff 3 (Table 3). However, p -value obtained by the independent sample t -test shows no statistical difference ($p > 5.0 \times 10^{-2}$) between them (this might be because extremely low TH-value in 3–14 largely affected p -value). The difference in TH-value between the backwall of tafoni and the cliff surface without tafoni is smaller in Cliffs 1 and 2 compared to Cliff 3. The value of TH differs with the amount of clay minerals contained in the rocks because seawater does not contain materials that affect the TH-value. The XRD patterns in Fig. 10 show that the rocks and precipitates on the studied cliffs have clay minerals such as clinoptilolite, garronite, phillipsite, and that the volume percentage of clinoptilolite must be much larger than the others. Other clay minerals, which might be formed through hydrothermal alteration or weathering, could also be present in the rocks and precipitates. However, their volume percentage would be too small to be detected in the XRD patterns as major components. Therefore, we consider that clinoptilolite is representative of the clay minerals in the rocks and precipitates, hence, TH-value is likely to be a proxy for clinoptilolite in this study. Thus, the amount of clinoptilolite must be larger on the surface of the tafoni than on the cliff surface without tafoni in Cliff 3.

The mean TOC content (wt%) is statistically lower in the backwall of tafoni than in the other parts of the Cliff 3 (Table 3). The difference is likely to be related to the precipitation of calcite on the backwall of tafoni. In Cliff 3, the results for the precipitates show that the flower-like part (No. 3-S1, S5, S7) is composed almost entirely of calcite because only carbon, a component of CaCO_3 , was detected. Both carbon and hydrogen are present in the precipitate without the flower-like structure (No. 3-S3, S4, S6, S8), indicating that it appears to be a mixture of calcite and clinoptilolite which is supported by XRD analysis (Fig. 10). Finally, what we can see on the backwall of tafoni, after the detachment of a gravel, without a particular expansion (e.g. No. 3-S2, S9) is not calcite and is entirely made of clinoptilolite. The above-mentioned results imply that these samples may show a process of precipitate growth on tafoni surface in Cliff 3; in other words, the difference in the shape of the precipitates reflects different degrees of growth, from appearance on the cliff surface to mature/expanded salt, along with a composition change from clinoptilolite to calcite. Therefore, the lower TOC-value in the backwall of tafoni is likely to indicate that carbon, most of which can originate from CO_2 in the air dissolved into the water, is removed from the surface for the precipitation of calcite.

Table 3
Summary of the results of the geochemical analyses.

Sample type	Surface	⁸⁷ Sr/ ⁸⁶ Sr	CHNS (wt%)			
			TN	TOC	TH	TS
Cliff 1						
Rock	<i>Without tafoni (n = 8)</i>					
	Maximum	0.708735	0.016	1.718	1.303	0.016
	Mean	0.706396	0.012	0.925	0.802	0.006
	Minimum	0.705187	0.010	0.189	0.012	0.000
	SD ^a	0.001583	0.003	0.766	0.692	0.009
	p-Value between tafoni		1.1 × 10 ⁻²	5.8 × 10 ⁻¹	6.7 × 10 ⁻¹	1.6 × 10 ⁻¹
Rock	<i>Tafoni (n = 3)</i>					
	Maximum	0.705597	0.005	1.196	1.484	0.380
	Mean	0.705367	0.004	0.604	1.015	0.180
	Minimum	0.705221	0.002	0.307	0.696	0.065
	SD ^a	0.000202	0.001	0.513	0.415	0.174
	p-Value between tafoni		N/A	N/A	N/A	N/A
Precipitate	<i>Tafoni (n = 6)</i>					
	Maximum	0.705244	0.007	3.108	2.563	0.219
	Mean	0.705233	0.006	1.056	2.118	0.117
	Minimum	0.705227	0.004	0.222	1.477	0.037
	SD ^a	0.000007	0.001	1.379	0.459	0.093
Cliff 2						
Rock	<i>Without tafoni (n = 8)</i>					
	Maximum	0.708589	0.012	0.807	1.245	0.131
	Mean	0.707727	0.004	0.276	0.750	0.046
	Minimum	0.706759	0.001	0.097	0.439	0.000
	SD ^a	0.000665	0.005	0.270	0.273	0.045
	p-Value between tafoni		4.0 × 10 ⁻¹	3.0 × 10 ⁻¹	9.3 × 10 ⁻¹	1.8 × 10 ⁻¹
Rock	<i>Tafoni (n = 3)</i>					
	Maximum	0.705998	0.002	0.114	0.850	0.269
	Mean	0.705770	0.002	0.095	0.766	0.126
	Minimum	0.705592	0.001	0.082	0.688	0.049
	SD ^a	0.000207	0.001	0.016	0.081	0.124
	p-Value between tafoni		N/A	N/A	N/A	N/A
Precipitate	<i>Tafoni (n = 3)</i>					
	Maximum	0.705812	0.006	0.003	2.811	0.433
	Mean	0.705706	0.005	0.002	2.364	0.235
	Minimum	0.705562	0.004	0.000	1.922	0.063
	SD ^a	0.000129	0.001	0.002	0.444	0.186
Cliff 3						
Rock	<i>Without tafoni (n = 4)</i>					
	Maximum	0.707044	0.020	0.508	0.924	0.189
	Mean	0.706039	0.008	0.263	0.578	0.068
	Minimum	0.705377	0.000	0.102	0.199	0.000
	SD ^a	0.000709	0.008	0.180	0.309	0.086
	p-Value between tafoni		7.7 × 10 ⁻¹	6.6 × 10 ⁻²	3.0 × 10 ⁻¹	7.2 × 10 ⁻¹
Rock	<i>Tafoni (n = 6)</i>					
	Maximum	0.705671	0.017	0.091	1.947	0.121
	Mean	0.705462	0.006	0.057	1.034	0.050
	Minimum	0.705312	0.001	0.009	0.135	0.000
	SD ^a	0.000146	0.007	0.035	0.747	0.051
	p-Value between tafoni		N/A	N/A	N/A	N/A
Precipitate	<i>Tafoni (n = 9)</i>					
	Maximum	0.706298	0.019	10.112	10.798	0.491
	Mean	0.705599	0.006	4.521	2.067	0.098
	Minimum	0.705343	0.000	0.000	0.000	0.000
	SD ^a	0.000293	0.008	3.882	3.422	0.171
Rock	<i>Transition zone (n = 3)</i>					
	Maximum	0.706110	0.028	0.363	0.692	0.042
	Mean	0.705856	0.021	0.281	0.658	0.027
	Minimum	0.705660	0.016	0.221	0.623	0.006
	SD ^a	0.000231	0.006	0.073	0.034	0.019
	p-Value between tafoni		3.7 × 10 ⁻²	2.8 × 10 ⁻³	4.4 × 10 ⁻¹	5.1 × 10 ⁻¹
Rock	<i>Bottom rim (n = 4)</i>					
	Maximum	0.708845	0.036	0.410	1.716	0.062
	Mean	0.708636	0.021	0.271	0.986	0.024
	Minimum	0.708333	0.003	0.067	0.582	0.004
	SD ^a	0.000242	0.017	0.147	0.506	0.026
	p-Value between tafoni		1.6 × 10 ⁻¹	3.0 × 10 ⁻²	9.2 × 10 ⁻¹	4.1 × 10 ⁻¹
Cliff 4						
Rock	<i>Without cave (n = 4)</i>					
	Maximum	0.707954				
	Mean	0.706635				
	Minimum	0.705726				

Table 3 (continued)

Sample type	Surface	⁸⁷ Sr/ ⁸⁶ Sr	CHNS (wt%)			
			TN	TOC	TH	TS
Rock	SD ^a	0.000944				
	Cave (n = 3)					
	Maximum	0.705393				
	Mean	0.705336				
	Minimum	0.705256				
Precipitate	SD ^a	0.000071				
	Cave (n = 5)					
	Maximum	0.705604				
	Mean	0.705403				
	Minimum	0.705268				
	SD ^a	0.000129				

^a SD: Standard deviation.

4.4. Moisture content

Hourly changes in w-value of the backwall of tafoni are shown in Fig. 11a, b, c and d. The w-value was higher in the morning and lower in the afternoon, and it decreased as the relative height of a measuring point increased. The range of moisture differences, which appears to reflect the amount of evaporation, also decreased as the relative height increased (Fig. 11a, b, d). These were common in all lines except for Line D (Fig. 11c). In Line D, the w-value and its range at 1 m were the lowest and the smallest, respectively.

Fig. 11e and f shows the averaged values of w measured at different parts of Cliffs 2 and 3. Lines C and D in Cliff 2 and Lines H and I in Cliff 3, which were set on tafoni, show higher moisture content than the other lines set on the cliff surface without tafoni. The effect of the measurement error on the results in Fig. 11 is negligible because the measurement error is smaller than ±2.5% of measurand (Matsukura and Takahashi, 1999).

4.5. Schmidt hammer rebound test

The results of the SH test are shown in Table 4 and Fig. 12. Fig. 12 shows the relationship between R_{max} and R_{min} during 20 impact repetitions for each test. In the result from Cliff 3, R_{max} and R_{min} are

plotted separately with location: the cliff surface without tafoni shows the lowest R_{max} and R_{min} values, and the backwall of tafoni shows the highest R_{max} and R_{min} values. The bottom rim has relatively smaller values than the backwall of tafoni. The plots for the transition zone appear to connect those for the backwall of tafoni to the cliff surface without tafoni, reflecting its spatial alignment on the cliff surface. However, no clear distinction of the plots is found in the results from Cliffs 1 and 2. We conducted independent sample t-test to evaluate the difference in R_{max} and R_{min} values between the backwall of tafoni and the other parts of the cliffs such as the cliff surface without tafoni, bottom rim and transition zone. The test statistically confirmed that the backwall of tafoni is harder than the other parts in Cliff 3 (Table 5). These results indicate that the physical and mechanical properties of the rocks differ with the locations in Cliff 3, whereas they are similar even in the different parts of the cliff surfaces in Cliffs 1 and 2.

5. Discussion

5.1. Essential factors for tafoni formation

Turkington and Paradise (2005) pointed out the importance of recognizing the system that controls weathering and the interactions

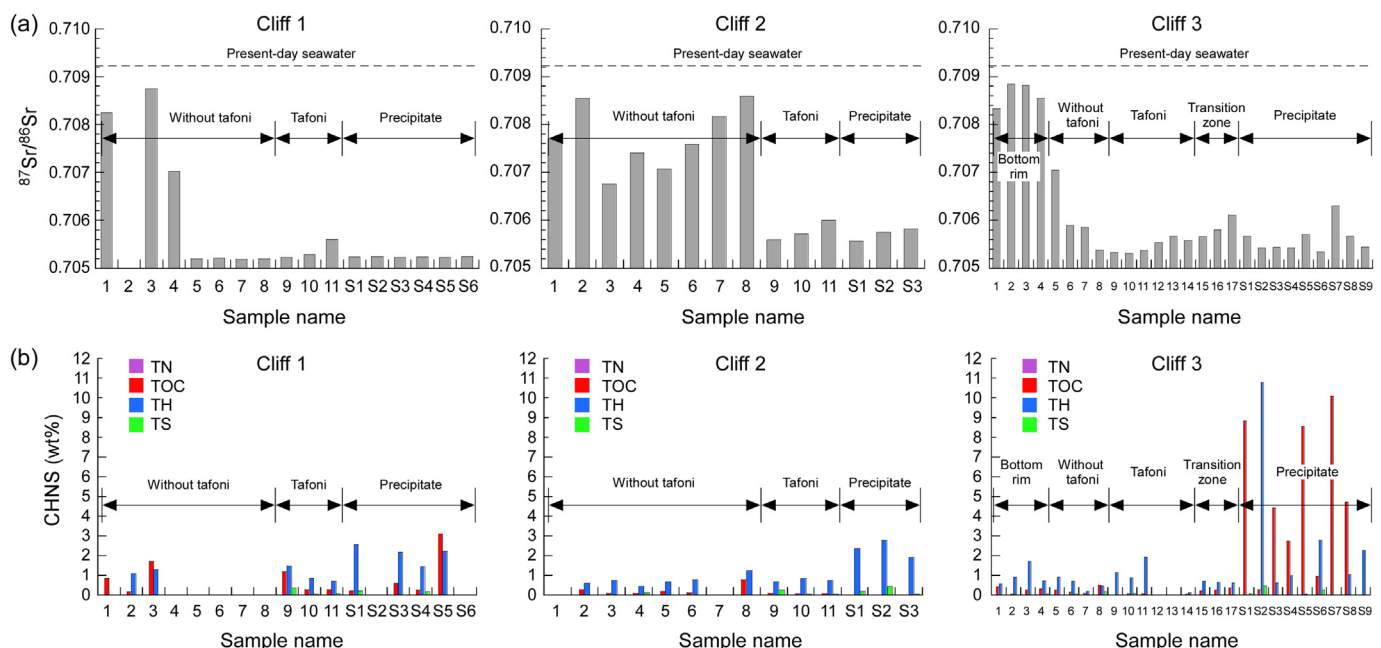


Fig. 9. Results of geochemical analyses: (a) ⁸⁷Sr/⁸⁶Sr ratio measurement and (b) CHNS elemental analysis.

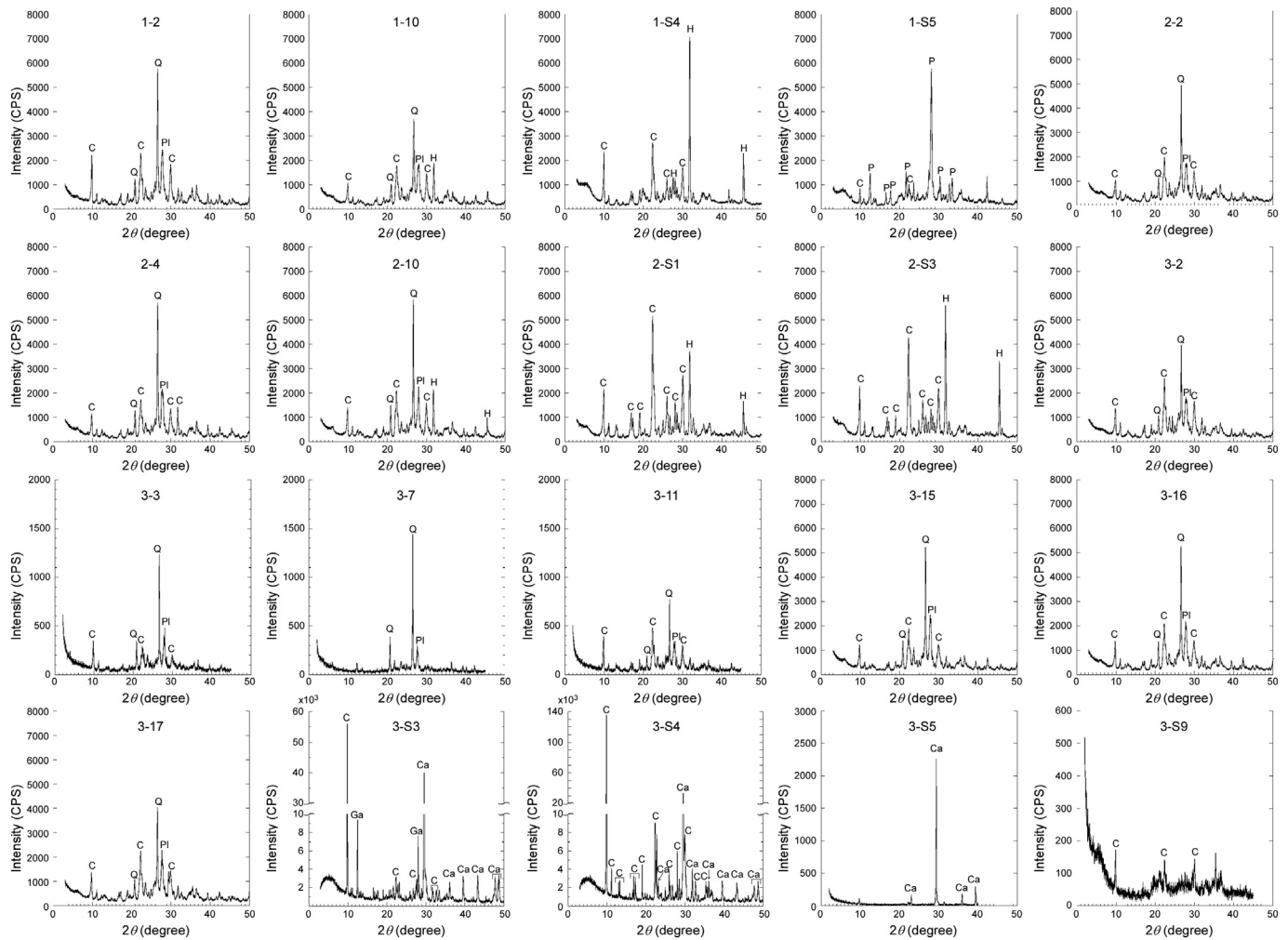


Fig. 10. X-ray diffraction patterns measured for the samples. The abbreviations “C”, “Ca”, “Ga”, “H”, “P”, “Pl” and “Q” denote clinoptilolite, calcite, garronite, halite, phillipsite, plagioclase and quartz, respectively.

between morphological elements, operating processes and environmental conditions. Bruthans et al. (2018) proposed a hierarchical model of interactions between the essential factors responsible for honeycomb formation. The model includes three factors: 1) initial and external factors; 2) organizing factors; and 3) decay factors. They mentioned that their model may be applicable to tafoni formation because the essential factors in the model are common between honeycombs and tafoni. Therefore, we apply this model to this study and discuss each factor to understand the tafoni formation process in a better way.

5.1.1. Initial factors

The initial and external factors via the hydraulic field dictate where salt precipitation and rock decay will occur and which surface morphology will be created (Bruthans et al., 2018). In addition to the initial rock shape, climate and vegetation (Bruthans et al., 2018), geological heterogeneities of rocks should be considered as initial factors in this study.

Rainwater could wash out surface materials of the cliffs including calcite and clinoptilolite and result in fewer precipitates on the cliff surface without tafoni than backwall of tafoni. However, rainwater is unlikely to be a main cause of the fewer precipitates. As seen on the backwall of tafoni (Fig. 5b), clinoptilolite or secondary calcite projecting from clinoptilolite can also be found on a depressed (sheltered in small scale) part of the cliff surface without tafoni if clinoptilolite content in the cliff surface without tafoni is same as that in the backwall of tafoni. This can be achieved even if most of clinoptilolite or calcite are removed by surface waterflow. However, the cliff surface without tafoni does not

include such clinoptilolite or calcite (Fig. 5c) unlike the backwall of tafoni (Fig. 5a and b). Furthermore, TH-content in the bottom rim of the tafoni in Cliff 3, where rainwater directly flow down similar to the cliff surface without tafoni, appears to be almost the same as that in the backwall of tafoni (Table 3 and Fig. 9b). This suggests that rainwater does not wash out clinoptilolite from the cliff surfaces. Therefore, it is reasonable to consider that clinoptilolite content is originally different between the cliff surface without tafoni and the backwall of tafoni.

Considering that clinoptilolite must have been formed during hydrothermal alteration prior to tafoni formation, the heterogeneity in the distribution of clinoptilolite was most likely to have been caused by the spatial alignment of flow path for hydrothermal alteration. Therefore, the distribution of flow paths was likely to work as the initial factor and controlled the distribution of clinoptilolite in this study. The flow paths include structural discontinuities such as bedding planes, faults, cracks and high-porosity zones without any discontinuities. The fluid behaviour in rock cores has been well visualized on a three-dimensional scale. A high-porosity zone, as revealed by medical X-ray computational tomography scanning, can be used as a flow path by any type of fluid (e.g., Kogure et al., 2017, 2018). Therefore, the porosity distribution can determine the configuration of the flow paths and result in heterogeneous distributions of secondary minerals. The higher *w*-value of the backwall of tafoni in Fig. 11e and f shows that the flow paths have still been used for the migration of water through the cliff body to the surface of the cliffs even in the present time.

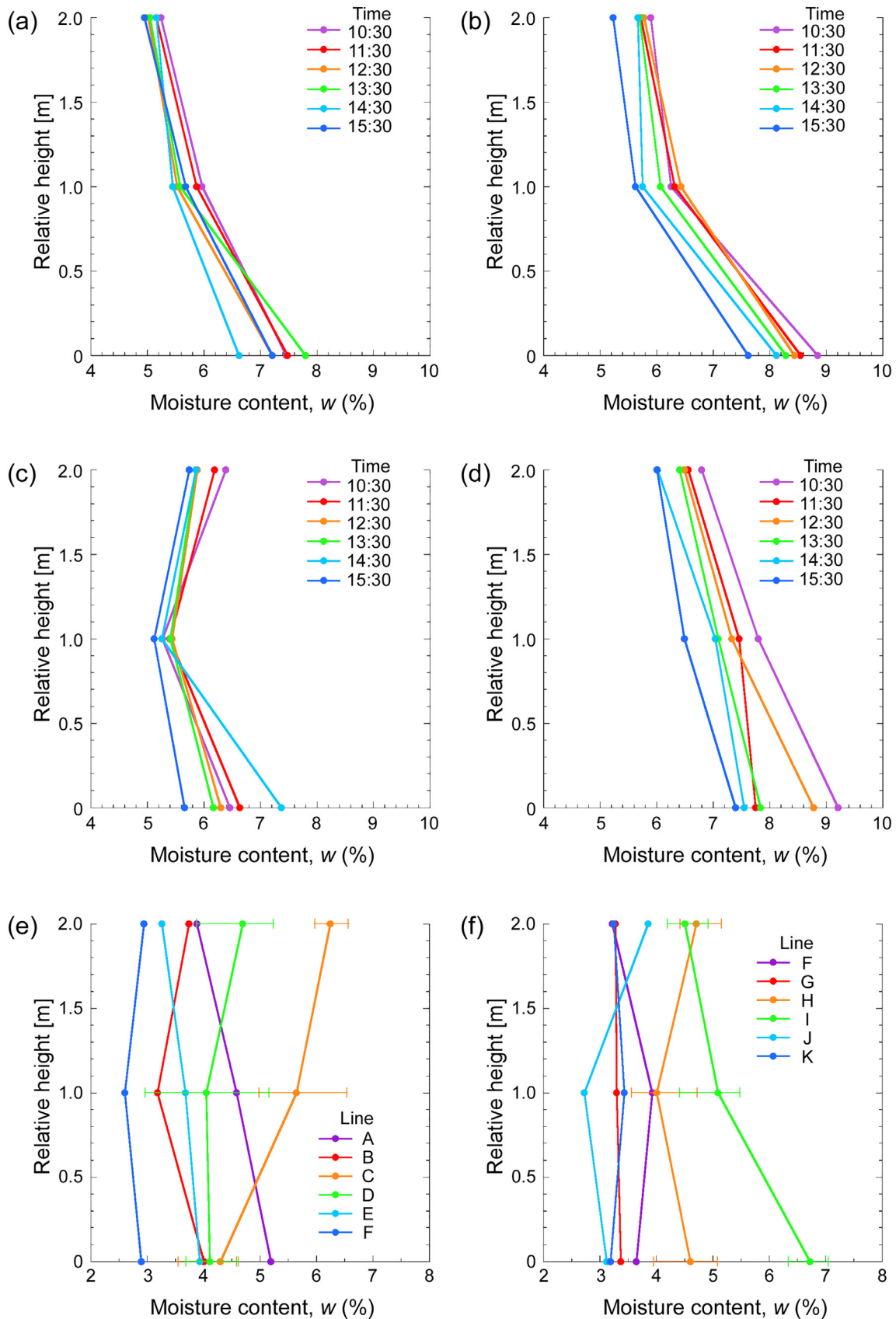


Fig. 11. Results of the changes in moisture content. Hourly changes in the backwall of tafoni in Cliff 3 along Lines (a) A, (b) C, (c) D and (d) E. Averaged moisture content around (e) Cliff 2 and (f) Cliff 3. An error bar shows the maximum and minimum values during the measurements. This figure is available in colour online.

Table 4
Results of the SH test.

No.	Surface	R_{max}	R_{min}
Cliff 1			
1	Without tafoni	48	18
2	ditto	52	12
3	ditto	47	16
4	ditto	42	21
5	ditto	55	29
6	ditto	53	12
7	Bottom rim	56	13
8	ditto	50	20
9	ditto	43	9
10	ditto	61	19
11	ditto	60	18
12	Without tafoni	56	11
13	ditto	45	17
14	Tafoni	32	13
15	ditto	41	20
16	ditto	44	14
17	ditto	50	20
18	ditto	44	21
19	ditto	42	13
20	ditto	50	23
21	ditto	50	34
22	ditto	41	15
23	ditto	64	37
Statistics			
p-Value between Tafoni and			
	Without tafoni	2.6×10^{-1}	2.8×10^{-1}
	Bottom rim	9.0×10^{-2}	2.3×10^{-1}
Cliff 2			
1	Without tafoni	37	12
2	ditto	36	13
3	ditto	42	12
4	ditto	43	18
5	Bottom rim	46	16
6	ditto	38	15
7	ditto	52	17
8	ditto	43	13
9	Without tafoni	41	18
10	ditto	40	12
11	ditto	53	12
12	ditto	37	18
13	ditto	33	12
14	ditto	39	9
15	ditto	59	17
16	Tafoni	43	20
17	ditto	52	14
18	ditto	35	16
19	ditto	44	9
20	ditto	56	14
21	ditto	48	16
22	ditto	46	14
23	ditto	50	16
24	ditto	53	9
Statistics			
p-Value between Tafoni and			
	Without tafoni	9.6×10^{-2}	8.4×10^{-1}
	Bottom rim	4.8×10^{-1}	5.9×10^{-1}
Cliff 3			
1	Bottom rim	55	13
2	ditto	53	29
3	ditto	57	9
4	ditto	46	12
5	ditto	48	9
6	ditto	47	12
7	ditto	53	11
8	ditto	48	9
9	ditto	52	28
10	Without tafoni	34	12
11	ditto	30	12
12	ditto	31	18
13	ditto	23	13
14	ditto	24	11
15	ditto	24	11
16	ditto	23	13

Table 4 (continued)

No.	Surface	R_{max}	R_{min}
17	ditto	24	11
18	ditto	20	12
19	ditto	20	10
20	Tafoni	52	30
21	ditto	60	20
22	ditto	62	31
23	ditto	60	30
24	ditto	60	17
25	Tafoni	62	21
26	ditto	56	16
27	ditto	57	22
28	ditto	56	25
29	ditto	64	24
30	ditto	57	34
31	ditto	60	30
32	Transition zone	51	19
33	ditto	48	30
34	ditto	58	23
35	ditto	58	28
36	ditto	38	21
Statistics			
p-Value between Tafoni and			
	Without tafoni	1.3×10^{-14}	2.9×10^{-6}
	Bottom rim	8.3×10^{-5}	2.9×10^{-3}
	Transition zone	8.8×10^{-3}	7.9×10^{-1}

R_{max} and R_{min} : maximum and minimum rebound value during 20 impacts.

Hydrothermal alteration can change the mechanical properties of a rock. Frolova et al. (2014) concluded that high-temperature fluids (>200 °C) cause consolidation and strengthening of rock and stated that this is the result of increased hardness developed by secondary minerals, such as zeolites and calcite, which fill pores and veins. Minerals that fill the intercrystalline and intergranular micropores make the largest contribution to rock strengthening, and the contacts between grains become stronger and denser, reinforcing the cementation of the rock (Frolova et al., 2014). Kogure et al. (2019) also reported that secondary carbonates filling pore spaces in sandstone result in an increase in UCS and radial compression strength. These processes seem to play a role in strengthening. Considering the similarity in the mineral components between these studies and the present study, these processes may also have occurred in the study cliffs, especially in Cliff 3: the backwall of tafoni in Cliff 3 has a greater hardness than the outer cliff surfaces, while no clear differences are found in Cliffs 1 and 2 (Table 5 and Fig. 12).

Hydrothermal alternation has also determined the distribution of clinoptilolite in addition to that of the R-value. To understand the relationship between the rock hardness and the amount of clinoptilolite, averaged R-values obtained from Cliffs 1, 2 and 3 (Table 5) were plotted against TH-values (Table 3). Fig. 13 shows a positive relationship between the parameters: the cliff surfaces become harder as the TH-value increases in any surface type. The data clearly show that hydrothermal alteration has worked as a principal initial factor for the surface topography of the study cliffs especially for Cliff 3. The role of hydrothermal alteration and its significance in salt weathering appear to have not been fully considered and recognized in the previous studies for tafoni formation on volcanic rocks (e.g. Höllermann, 1975; Kelletat, 1980).

The difference in the clinoptilolite content possibly produced by the following factors. Firstly, it is related to the amount of glass in the pyroclastic rocks since, within the minerals in the rocks, glass is subject to hydrothermal alteration easily (e.g. Browne, 1978). Glass alters to other minerals including zeolite series. Therefore, a part of Cliff 3 with high clinoptilolite content could have originally been rich in glass. The second factor is the difference in the degree of hydrothermal alteration with location. Fig. 13 supports the second factor because higher hydrothermal alternation increases both clinoptilolite content and rock hardness. Volcanic hydrothermal circulation is controlled by the architecture

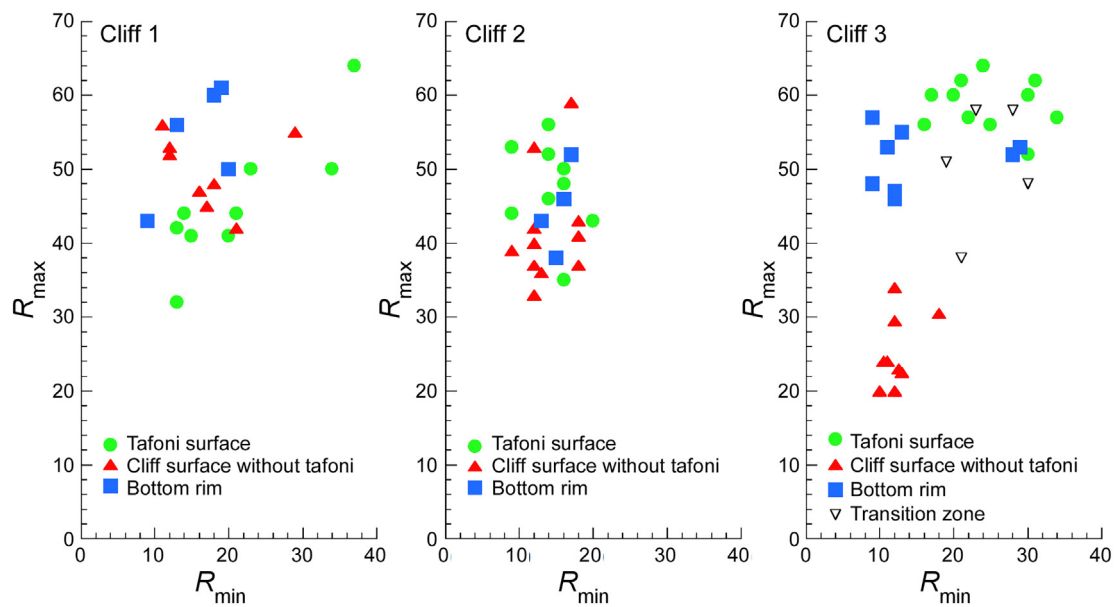


Fig. 12. Results of the SH test showing the relationship between R_{\max} and R_{\min} . This figure is available in colour online.

of original volcanoes: strong hydrothermal alteration is usually limited to areas close to dikes, sills, subvolcanic intrusive rocks and vent structures (e.g., Van Kranendonk, 2006). These structures, which originated from previous volcanic activity after the opening of the Sea of Japan, are well preserved in some areas around the Shimane Peninsula (Kano et al., 1993). Considering that the geochemical and mechanical properties of the rock surfaces gradually change within a few metres in the transition zone in Cliff 3, the transition zone appears to be a boundary between the rocks with strong hydrothermal alteration and those with less alteration. Therefore, a specific volcanic architecture is likely to exist close to the tafoni as evidence of hydrothermal circulation, although the tafoni surface itself does not show such distinctive features.

5.1.2. External factors

External factors that should be considered in this study include climate and seawater. Although Ohda City is located in a humid subtropical area, there were dozens of days on which temperatures dropped below 0 °C (Fig. 2b). The effect of freezing and thawing on tafoni formation has been reported in cold regions such as Finland (Kejonen et al., 1988) and Antarctica (e.g., Hall and André, 2006). However, even in Antarctica, freezing is not necessarily a main cause of tafoni formation (Prebble, 1967; Strini et al., 2008). Cárdenes et al. (2014) conducted laboratory experiments on the durability of sedimentary rocks against salt crystallization and freeze-thaw cycles and concluded that salt crystallization has more devastating effects than freeze-thaw cycles in most cases. These studies imply that the freeze-thaw process is effective only under limited environmental conditions. Considering that the coastal area is usually warmer than inland area at night, actual nighttime low temperature around the study cliffs is likely to be higher than the one measured at the weather station representative for Ohda city (Fig. 2). This is because the coastal cliffs locate 5 km away from the station. This suggests that imperceptible freeze-thaw process would operate on the backwall of tafoni and the cliff surfaces without tafoni only for a limited duration in a year. Therefore, the contribution of the freeze-thaw process to tafoni formation in the study cliffs is likely to be very small.

Seawater could also be responsible for tafoni development in the coastal areas as a source of salts (e.g., Mottershead and Pye, 1994). In the study site, seawater is likely to contribute to tafoni formation in Cliffs 1 and 2 through the precipitation of halite (Fig. 10). On the other hand, the results of $^{87}\text{Sr}/^{86}\text{Sr}$ measurements clearly show that the

source of Ca is not seawater but clinoptilolite in cliff materials in Cliff 3. Calcite precipitates from the water from the rock interior (e.g., Schweigstillová et al., 2009; Navrátil et al., 2013) in Cliff 3.

5.1.3. Organizing factors

Organizing factors such as the hydraulic field and its boundary conditions have crucial controls on the location of the salt decay zone whenever salt precipitates from capillary water migrating through a rock body (Bruthans et al., 2018). The hydraulic field is composed of the capillary zone, where liquid water is transported by capillary pressure inside the rock body, and the vapor zone, where only water vapor is transported (Fig. 1 in Bruthans et al., 2018). The contact of both zones where salt precipitates is called the evaporation zone. The salt decay zone therefore seems to be the same as the evaporation zone. The boundary conditions are determined by the microclimate, i.e., the balance between the infiltration of water and potential evaporation.

Our measurements revealed that Ca in clinoptilolite dissolves into freshwater. Dissolved Ca precipitates as secondary calcite when the freshwater evaporates in the salt decay zone. Bruthans et al. (2018) showed two types of tafoni formation models depending on the depth of the salt decay zone determined by the balance between the evaporation rate and the infiltration/recharge rate of water. The salt decay zone exists close to the rock surface if the depth of the hydraulic potential field is close to the surface, and vice versa. In their model, cavernous weathering will proceed if the salt decay zone exists in the deeper zone because salts are deposited in pits. On the other hand, the salt decay zone located close to the rock surface results in salt deposition in lips and their gradual destruction and smoothing of the surface.

There are some holes in the cliff surfaces surrounding the upper part of the tafoni in Cliff 2 and Cliff 3 (Fig. 3b, c), which seem to have coalesced to become larger. The coalescence of cavernous structures occurs during their evolution processes (e.g., Mustoe, 1983; McBride and Picard, 2000; Chen et al., 2019). Tafoni and honeycombs increase their depth and width simultaneously and then develop laterally when their sidewalls are breached (McBride and Picard, 2000; Chen et al., 2019). However, the holes in this study appear to have no sidewalls and are connected to the large hollows just beneath the cliff surface surrounding the tafoni (Fig. 5). The surface is actually just a thin crust with some holes. This indicates that the salt decay zone and the evaporation

Table 5
Summary of the results of the SH test.

Surface type (Number of SH test)	R_{max}	R_{min}
Cliff 1		
<i>Without tafoni (n = 8)</i>		
Maximum	56	29
Mean	49.8	17.0
Minimum	42	11
SD ^a	5.0	6.0
p-Value between tafoni	2.6×10^{-1}	2.8×10^{-1}
<i>Bottom rim (n = 5)</i>		
Maximum	61	20
Mean	54.0	15.8
Minimum	43	9
SD ^a	7.5	4.7
p-Value between tafoni	9.0×10^{-2}	2.3×10^{-1}
<i>Tafoni (n = 10)</i>		
Maximum	64	37
Mean	45.8	21.0
Minimum	32	13
SD ^a	8.4	8.5
p-Value between tafoni	N/A	N/A
Cliff 2		
<i>Without tafoni (n = 11)</i>		
Maximum	59	18
Mean	41.8	13.9
Minimum	33	9
SD ^a	7.7	3.2
p-Value between tafoni	9.6×10^{-2}	8.4×10^{-1}
<i>Bottom rim (n = 4)</i>		
Maximum	52	17
Mean	44.8	15.3
Minimum	38	13
SD ^a	5.9	1.7
p-Value between tafoni	4.8×10^{-1}	5.9×10^{-1}
<i>Tafoni (n = 9)</i>		
Maximum	56	20
Mean	47.4	14.2
Minimum	35	9
SD ^a	6.3	3.5
p-Value between tafoni	N/A	N/A
Cliff 3		
<i>Without tafoni (n = 10)</i>		
Maximum	34	18
Mean	25.2	12.2
Minimum	20	10
SD ^a	4.6	2.2
p-Value between tafoni	1.3×10^{-14}	2.9×10^{-6}
<i>Bottom rim (n = 9)</i>		
Maximum	57	29
Mean	51.0	14.7
Minimum	46	9
SD ^a	3.9	8.0
p-Value between tafoni	8.3×10^{-5}	2.9×10^{-3}
<i>Tafoni (n = 12)</i>		
Maximum	64	34
Mean	58.8	25.0
Minimum	52	16
SD ^a	3.3	5.9
p-Value between tafoni	N/A	N/A
<i>Transition zone (n = 5)</i>		
Maximum	58	30
Mean	50.6	24.2
Minimum	38	19
SD ^a	8.3	4.7
p-Value between tafoni	8.8×10^{-3}	7.9×10^{-1}

^a SD: Standard deviation.

front are likely to exist deeper from the surfaces, organizing the cavernous structure beneath the cliff surfaces in the study cliffs.

5.1.4. Decay factors

Our investigations show that the dominant decay factor for tafoni is the precipitation of halite for Cliffs 1 and 2 and calcite for Cliff 3. The pressure induced by salt crystallization in confinement was measured

by laboratory experiments although salt damage mechanisms are complex (Goudie and Viles, 1997). Desarnaud et al. (2016) measured the force exerted by growing alkali halide salt crystals while visualizing their spontaneous nucleation and growth. The maximum pressure of NaCl (halite) varies from approximately 100 to 1000 MPa depending on the degree of salt concentration. The crystallization pressure of sodium sulfate, Na₂SO₄, was determined to be 200–350 MPa (Saidov et al., 2015). These studies indicate that the crystallization pressure is on the order of 100 MPa, although to the best of our knowledge, studies on CaCO₃ have not been performed. The rock strength of the study cliffs can be determined by converting the R-value in the SH test. Considering that the rock body will be ruptured by the increased volume of calcite inside the rock, the tensile strength (S_t) of the rock should be compared with the crystallization pressure. The maximum value of R_{max} in the backwall of tafoni is 64 in Cliff 3 between the studied cliffs (Table 5), which equals a UCS of 228 MPa according to a conversion chart attached to the instrument used for the test. Value of S_t can be estimated from the UCS because the UCS is 5–25 times larger than the S_t in many rocks (Sunamura, 1992). This consistency allows us to estimate that the maximum S_t is approximately 45 MPa. Therefore, it is plausible that the crystallization pressure of halite and calcite exceeds the S_t of the rock, which is sufficient to induce salt weathering.

The numerical simulation by Huinink et al. (2004) showed that most salts should be deposited at places with maximum evaporation. In the studied cliffs, as far as we can understand, the maximum evaporation from the backwall of tafoni is likely to occur at the measurement points that correspond to the retreat points of each measurement line in Cliff 3 where the highest moisture content and the maximum range of the moisture difference were found: the retreat point is at the relative height of 2 m in Cliff 2 (Lines C and D in Fig. 11e) and of 0 m in Cliff 3 (Fig. 11a, b, c, d, and Lines H and I in Fig. 11f). Therefore, salt weathering on the backwall of tafoni is likely to be controlled by evaporation processes. Huinink et al. (2004) showed that a long drying period is important for tafoni development, and this is more likely to occur at the more sheltered parts of a rock surface. Schnepfleitner et al. (2016) pointed out that this mechanism is responsible for the tendency of tafoni to grow upward because the upper part of tafoni has sheltered parts that receive no direct sunlight in many cases, resulting in higher moisture contents than the parts with direct sunlight. In this study, the cliff surface surrounding the upper part of the tafoni has hollows beneath the surface, while no hollows have developed on the sidewall of the tafoni

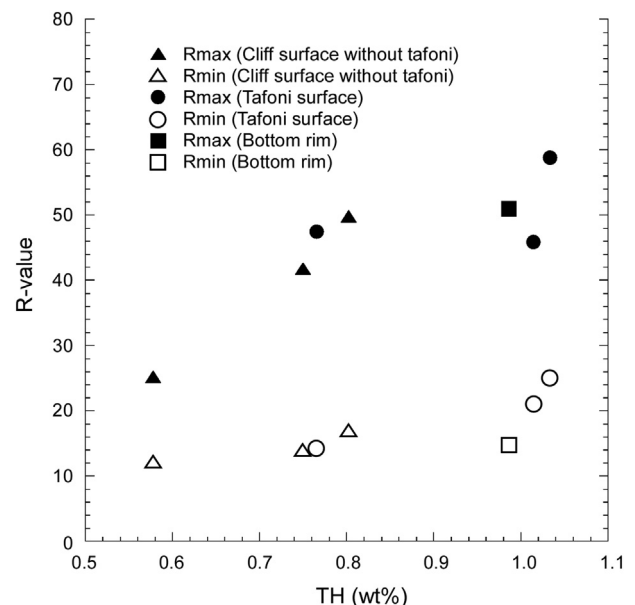


Fig. 13. Relationship between R-value and TH in the cliff surfaces.

(Figs. 3a, b, 4c and d). The moisture content in the sheltered hollows must be larger with slower drying phases than the other parts, although we have no quantitative data at the present moment.

5.2. Formation process of surface topography of Cliff 3

We consider that the formation process of tafoni and the surface topography in Cliff 3 is unique compared to the other studied cliffs and previous studies. The formation process is summarized in the following statements. The process is divided into two patterns according to the amount of clinoptilolite present in the rocks: one is associated with tafoni (Fig. 14a), and the other is associated with rockfalls (Fig. 14b). In the cliff with tafoni, much calcium released from clinoptilolite dissolves into freshwater that migrates through the cliff as capillary flow. Freshwater may consist of rainwater and groundwater; however, only rainwater is illustrated in the figure because we have no information on the presence of groundwater. Calcite precipitates when freshwater reaches across the border to the vapor zone for evaporation. Calcite precipitation facilitates salt weathering of the cliff surface to form tafoni. Therefore, the locations of tafoni are likely to correspond to cliff surfaces rich in clinoptilolite. Both the higher strength of the backwall of tafoni and the disintegration of the backwall surface into small particles caused by frequent salt weathering may have led to the prevention of the rockfalls as seen in the cliff surface without tafoni.

The tafoni depth is larger in the lower part of the cliff where the moisture content is higher, and larger fluctuations were measured (Fig. 11). It is predictable that the rainwater that infiltrated from the top surface migrates downward through the cliff body by gravity. In

addition, rainwater migrates laterally from inside the cliff towards the cliff surface because of the gradient in water pressure (Schnepfleitner et al., 2016). Therefore, the balance between the rate of downward and lateral migration of freshwater is likely to control the height of the higher moisture part, which results in the larger tafoni depth (Fig. 14a). The salt concentration in the sheltered part of the upper part of the cliffs is found to form hollows just beneath the surface. The longer drying period in the sheltered part promotes the precipitation of calcite, although the volume of Ca-containing rainwater provided to the sheltered part must be smaller than that provided to the lower part. Therefore, the study cliffs have two active parts for tafoni formation that are possibly produced by different hydrological and evaporation processes.

The cliff associated with rockfalls (Fig. 14b) has a smaller amount of clinoptilolite than the cliff with tafoni (Tables 2 and 3). The concentration of Ca dissolved into the rainwater must be so small that calcite does not precipitate on the cliff surface (Fig. 5c). The cliff surface with smaller R-values is then likely to become the source of rockfalls. Based on these processes, the identification of potential rockfalls is likely achieved by the presence or absence of tafoni in the study site.

Finally, we emphasize that rockfalls from the cliff surfaces with/without tafoni discussed in this study are different from the collapse of a visor, which is a part of the cliff surface surrounding the tafoni. It is known that visors surrounding cavernous decay (including notches) become unstable and collapse as the decay grows (e.g., McBride and Picard, 2000; Kogure et al., 2006; Shtober-Zisu et al., 2017). Therefore, collapses of the visors can also occur in the study area when the gravitational forces affecting the visors exceed the S_t of the cliff materials (e.g., Kogure et al., 2006). However,

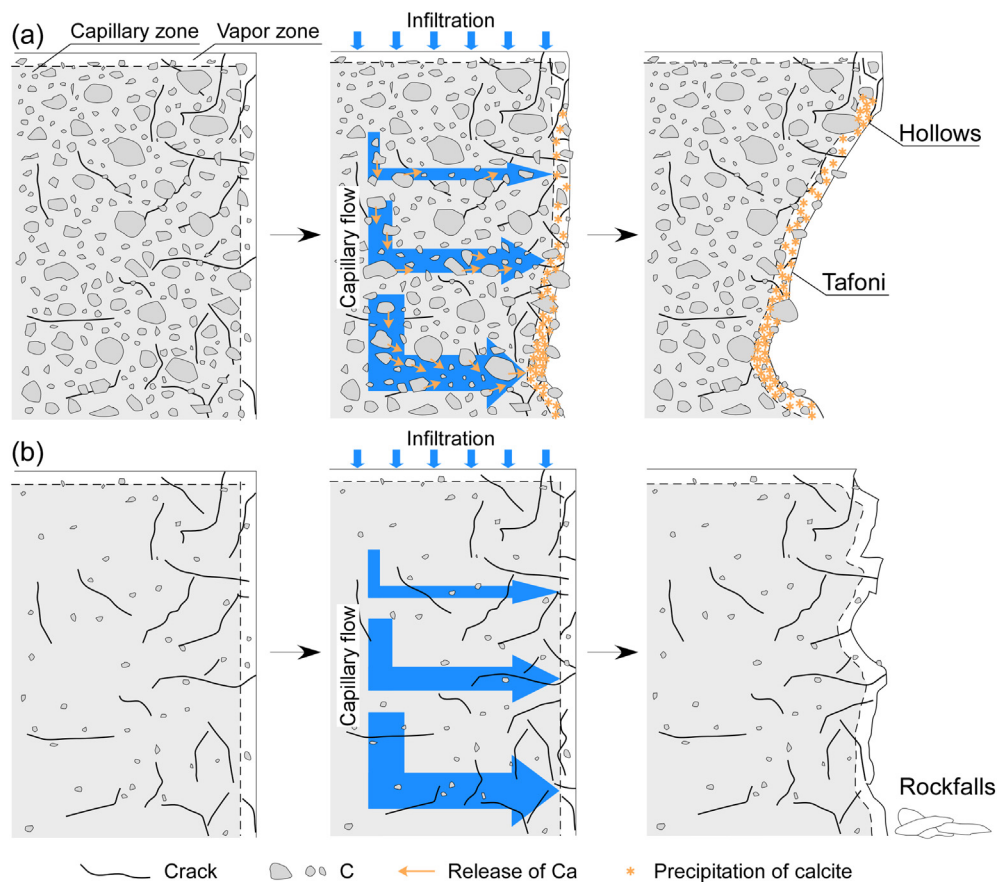


Fig. 14. Schematic diagrams of the differing processes of (a) tafoni formation and (b) rockfall in Cliff 3. The abbreviations “C” and “Ca” denote clinoptilolite and calcite, respectively. This figure is available in colour online.

there are no rock masses at the base of the tafoni (Fig. 4), including those that can be clearly identified as a part of the visors. This indicates that visor collapses are unlikely to occur or that the visors gradually disintegrate into materials consisting of rhyolitic pyroclastic rock, although detailed processes are not obvious. It can also be supposed that the visors actually collapse, and fallen visors are removed by waves immediately after collapse.

6. Conclusions

This study discussed the factors and processes for the origin and development of tafoni on the coastal cliff surfaces in Shimane, Japan. Geochemical analyses were conducted to elucidate the origin of the Ca in the rocks and precipitates and to evaluate the amount of clinoptilolite, which is directly related to the presence of Ca. The SH test was also applied to the surface of the cliffs to determine the physical and mechanical properties of the surfaces.

The results revealed that localized hydrothermal alteration was an important prerequisite to promote subsequent tafoni formation in addition to the salt weathering process caused by halite precipitation which is well known in coastal environment. The hydrothermal alteration produced a substantial amount of clinoptilolite and induced strengthening of the rock. Eventually, the crystallization pressure of calcite originating from clinoptilolite exceeds even the tensile strength of the strengthened surface to form tafoni. The specific conclusions are as follows:

- (1) The CHNS analyses and XRD patterns show that the rocks and precipitates on the studied cliffs contain clay minerals, most of which are clinoptilolite with Ca as a main component. It also noted that calcite occurs on the backwall of the largest tafone in the hardest surface within the studied cliffs whereas halite occurs on that with relatively lower hardness.
- (2) In any surface type, the hardness of the cliff and tafoni surfaces increases as the clinoptilolite content increases, indicating that a higher degree of hydrothermal alteration results in higher strength.
- (3) More clay minerals are present especially in the backwall of the largest tafone than in those without tafoni.
- (4) The measurements of the $^{87}\text{Sr}/^{86}\text{Sr}$ ratio for the rocks and precipitates reveal that the Ca in the precipitates does not originate from seawater, instead it derives from the cliff materials. This observation indicates that clinoptilolite is the source of Ca in the calcite that precipitated on the tafone.
- (5) Tafoni mainly forms through salt weathering by calcite precipitation on the sites with higher effect of hydrothermal alteration. On the other hand, tafoni develop by halite precipitation, if the cliffs had been less affected by hydrothermal alteration and receive more amount of seawater through splashing.

The locations of the tafoni with harder surfaces therefore appears to cover areas where the effect of hydrothermal alteration was higher. Whereas rockfalls occur in areas less affected by hydrothermal alteration. The presence of tafoni indicates a low risk of rockfalls. This information will be useful for disaster prevention.

Data availability

Data to illustrate XRD patterns of the samples are available from the following link: <https://doi.org/10.6084/m9.figshare.14245745>.

Declaration of competing interest

The authors declare that they have no known competing financial interests or personal relationships that could have appeared to influence the work reported in this paper.

Acknowledgements

This study was partly supported by JSPS KAKENHI Grant Number 15H05350 and Joint Research Grant for the Environmental Isotope Study of Research Institute for Humanity and Nature through TK. This manuscript has been much improved by comments and suggestions from two anonymous reviewers.

References

- Aydin, A., Basu, A., 2005. The Schmidt hammer in rock material characterization. *Eng. Geol.* 81, 1–14. <https://doi.org/10.1016/j.enggeo.2005.06.006>.
- Browne, P.R.L., 1978. Hydrothermal alteration in active geothermal fields. *Annu. Rev. Earth Planet. Sci.* 6, 229–250.
- Bruthans, J., Filippi, M., Slavík, M., Svobodová, E., 2018. Origin of honeycombs: testing the hydraulic and case hardening hypotheses. *Geomorphology* 303, 68–83. <https://doi.org/10.1016/j.geomorph.2017.11.013>.
- Cárdenes, V., Mateos, F.J., Fernández-Lorenzo, S., 2014. Analysis of the correlations between freeze–thaw and salt crystallization tests. *Environ. Earth Sci.* 71, 1123–1134. <https://doi.org/10.1007/s12665-013-2516-7>.
- Chen, L.Q., Guo, F.S., Liu, F.J., Xu, H., Ding, T., Liu, X., 2019. Origin of Tafoni in the Late Cretaceous Aeolian Sandstones, Danxia Shan UNESCO Global Geopark, South China. *Acta Geol. Sin.-Engl. Ed* 93, 451–463. <https://doi.org/10.1111/1755-6724.13810>.
- Committee, Analytical Methods, 2006. Evaluation of analytical instrumentation. Part XIX CHNS elemental analysers. *Accredit. Qual. Assur.* 11, 569–576. <https://doi.org/10.1007/s00769-006-0185-x>.
- Conca, J.L., Rossman, G.R., 1982. Case hardening of sandstone. *Geology* 10, 520–523. [https://doi.org/10.1130/0091-7613\(1982\)10<520:CHOS>2.0.CO;2](https://doi.org/10.1130/0091-7613(1982)10<520:CHOS>2.0.CO;2).
- Conca, J.L., Rossman, G.R., 1985. Core softening in cavernously weathered tonalite. *J. Geol.* 93, 59–73. <https://doi.org/10.1086/628919>.
- Coombs, D.S., Ellis, A.J., Fyfe, W.S., Taylor, A.M., 1959. The zeolite facies, with comments on the interpretation of hydrothermal syntheses. *Geochim. Cosmochim. Acta* 17. [https://doi.org/10.1016/0016-7037\(59\)90079-1](https://doi.org/10.1016/0016-7037(59)90079-1) 573–107.
- Coombs, D.S., Alberti, A., Armbruster, T., Artioli, G., Colella, C., Galli, E., Grice, J.D., Liebau, F., Mandarino, J.A., Minato, H., Nickel, E.H., Passaglia, E., Peacor, D.R., Quartieri, S., Rinaldi, R., Ross, M., Sheppard, R.A., Tillmanns, E., Vezzalin, G., 1997. Recommended nomenclature for zeolite minerals: report of the subcommittee on zeolites of the International Mineralogical Association, Commission on New Minerals and Mineral Names. *Can. Mineral.* 35, 1571–1606.
- Desarnaud, J., Bonn, D., Shahidzadeh, N., 2016. The pressure induced by salt crystallization in confinement. *Sci. Rep.* 6, 30856. <https://doi.org/10.1038/srep30856>.
- Eklund, J.A., Zhang, H., Viles, H.A., Curteis, T., 2013. Using handheld moisture meters on limestone: factors affecting performance and guidelines for best practice. *Int. J. Archit. Herit.* 7, 207–224. <https://doi.org/10.1080/15583058.2011.626491>.
- Elderfield, H., 1986. Strontium isotope stratigraphy. *Paleogeogr. Paleoclimatol. Paleocol.* 57, 71–90. [https://doi.org/10.1016/0031-0182\(86\)90007-6](https://doi.org/10.1016/0031-0182(86)90007-6).
- Faure, G., Mensing, T.M., 2004. *Isotopes, Principles and Applications*. 2nd ed. John Wiley & Sons Inc, New Jersey.
- Frolova, J., Ladygin, V., Rychagov, S., Zukhubaya, D., 2014. Effects of hydrothermal alterations on physical and mechanical properties of rocks in the Kuril-Kamchatka island arc. *Eng. Geol.* 183, 80–95. <https://doi.org/10.1016/j.enggeo.2014.10.011>.
- Goudie, A.S., Viles, H., 1997. *Salt Weathering Hazards*. John Wiley & Sons, Chichester.
- Goudie, A.S., Migoñ, P., Allison, R.J., Rosser, N., 2002. Sandstone geomorphology of the Al-Quwayra area of South Jordan. *Zeitschrift für Geomorphol.* 46, 365–390. <https://doi.org/10.1127/zfg/46/2002/365>.
- Hall, K., André, M.-F., 2006. Temperature observations in Antarctic tafoni: implications for weathering, biological colonization, and tafoni formation. *Antarct. Sci.* 18, 377–384. <https://doi.org/10.1017/S0954102006000423>.
- Höllermann, P., 1975. Formen Kaverner Verwitterung (“Tafoni”) Auf Teneriffa. *Catena* 2, 385–409. [https://doi.org/10.1016/S0341-8162\(75\)80024-5](https://doi.org/10.1016/S0341-8162(75)80024-5).
- Huinink, H.P., Pel, L., Kopinga, K., 2004. Simulating the growth of tafoni. *Earth Surf. Process. Landf.* 29, 1225–1233. <https://doi.org/10.1002/esp.1087>.
- Iizumi, S., Otani, S., Hara, K., 1999. Sr and Nd isotope ratios of Middle Miocene volcanic rocks from Shimane Peninsula, San’in district, Southwest Japan. *Mem. Geol. Soc. Japan.* 53, 383–391.
- Japan Meteorological Agency. (Accessed 19 March 2021).
- Kano, K., Yamaoto, T., Takeuchi, K., 1993. A Miocene island-arc volcanic seamount: the Takashibiyama Formation, Shimane Peninsula, SW Japan. *J. Volcanol. Geotherm. Res.* 59, 101–119. [https://doi.org/10.1016/0377-0273\(93\)90080-B](https://doi.org/10.1016/0377-0273(93)90080-B).
- Kano, K., Matsuura, H., Sawada, Y., Takeuchi, K., 1998. *Geology of the lawami-Ōda and Ōura Districts With Geological Sheetmap at 1:50000*. Geological Survey of Japan, Tsukuba (in Japanese with English abstract).
- Kejonen, A., Kielosto, S., Lahti, S.I., 1988. Cavernous weathering forms in Finland. *Geogr. Ann.* 70, 315–321. <https://doi.org/10.1080/04353676.1988.11880262>.
- Kelletat, D., 1980. Studies on the age of honeycombs and tafoni features. *Catena* 7, 317–325. [https://doi.org/10.1016/0341-8162\(80\)90016-8](https://doi.org/10.1016/0341-8162(80)90016-8).
- Kogure, T., 2019. Analysis of Schmidt hammer rebound test results with repetitive impacts for determining the mechanical characteristics of weathered pyroclastic rock surfaces: a case study along the Isotake coast, Japan. *Bull. Eng. Geol. Environ.* 78, 3425–3432. <https://doi.org/10.1007/s10064-018-1334-2>.
- Kogure, T., Aoki, H., Maekado, A., Hirose, T., Matsukura, Y., 2006. Effect of the development of notches and tension cracks on instability of limestone coastal cliffs in the Ryukyus,

- Japan. *Geomorphology* 80, 236–244. <https://doi.org/10.1016/j.geomorph.2006.02.012>.
- Kogure, T., Zhang, Y., Nishizawa, O., Xue, Z., 2017. Migration mode of brine and supercritical CO₂ during steady-state relative permeability measurements at very slow fluid flow velocity. *Geophys. J. Int.* 211, 1237–1253. <https://doi.org/10.1093/gji/ggx335>.
- Kogure, T., Zhang, Y., Nishizawa, O., Xue, Z., 2018. Changes in migration mode of brine and supercritical CO₂ in imbibition process under steady flow state of very slow fluid velocities. *Geophys. J. Int.* 214, 1413–1423. <https://doi.org/10.1093/gji/ggy210>.
- Kogure, T., Naka, Y., Sasaki, K., Endo, S., 2019. Physical and mechanical properties of sandstone and calcareous concretions at the wave-cut bench in Iwami-tatamigaura, a natural monument in Shimane, Japan. *J. Japan Soc. Eng. Geol.* 59, 446–452. <https://doi.org/10.5110/jjseg.59.446> (in Japanese with English abstract).
- Lea, D.W., Mashiotta, T.A., Spero, H.J., 1999. Controls on magnesium and strontium uptake in planktonic foraminifera determined by live culturing. *Geochim. Cosmochim. Acta* 63, 2369–2379. [https://doi.org/10.1016/S0016-7037\(99\)00197-0](https://doi.org/10.1016/S0016-7037(99)00197-0).
- Martinho, E., Alegria, F., Dionísio, A., Grangeia, C., Almeida, F., 2012. 3D-resistivity imaging and distribution of water soluble salts in Portuguese Renaissance stone bas-reliefs. *Eng. Geol.* 141–142, 33–44. <https://doi.org/10.1016/j.enggeo.2012.04.010>.
- Matsukura, Y., Aoki, H., 2004. The Schmidt hammer: a brief review and some problems in geomorphology. *Trans. Japan. Geomorph. Union* 25, 175–196 (in Japanese with English abstract).
- Matsukura, Y., Takahashi, K., 1999. A new technique for rapid and non-destructive measurement of rock-surface moisture content; preliminary application to weathering studies of sandstone blocks. *Eng. Geol.* 55, 113–120. [https://doi.org/10.1016/S0013-7952\(99\)00111-8](https://doi.org/10.1016/S0013-7952(99)00111-8).
- Matsukura, Y., Tanaka, Y., 2000. Effect of rock hardness and moisture content on tafoni weathering in the granite of Mount Doeg-sung, Korea. *Geogr. Ann.* A 82, 59–67. <https://doi.org/10.1111/j.0435-3676.2000.00112.x>.
- McBride, E.F., Picard, M.D., 2000. Origin of development of tafoni in Tunnel Spring Tuff, Crystal Peak, Utah, USA. *Earth Surf. Process. Landf.* 25, 869–879. [https://doi.org/10.1002/1096-9837\(200008\)25:8<869::AID-ESP104>3.0.CO;2-F](https://doi.org/10.1002/1096-9837(200008)25:8<869::AID-ESP104>3.0.CO;2-F).
- Mellor, A., Short, J., Kirkby, S.J., 1997. Tafoni in the El Chorro area, Andalucía, southern Spain. *Earth Surf. Process. Landf.* 22, 817–833. [https://doi.org/10.1002/\(SICI\)1096-9837\(199709\)22:9<817::AID-ESP768>3.0.CO;2-T](https://doi.org/10.1002/(SICI)1096-9837(199709)22:9<817::AID-ESP768>3.0.CO;2-T).
- Misumi, H., Ohira, H., 2006. Zeolite alteration and fission track ages reported from Ootacity, Shimane Prefecture, SW Japan. *Fission Track News Lett.* 19, 19–23 (in Japanese with English abstract).
- Mottershead, D.N., Pye, K., 1994. Tafoni on coastal slopes, South Devon, U.K. *Earth Surf. Process. Landf.* 19, 543–563. <https://doi.org/10.1002/esp.3290190607>.
- Mustoe, G.E., 1983. Cavernous weathering in the Capitol Reef Desert, Utah. *Earth Surf. Process. Landf.* 8, 517–526. <https://doi.org/10.1002/esp.3290080603>.
- Mustoe, G.E., 2010. Biogenic origin of coastal honeycomb weathering. *Earth Surf. Process. Landf.* 424–434. <https://doi.org/10.1002/esp.1931>.
- Navrátil, T., Vařilová, Z., Rohovec, J., 2013. Mobilization of aluminum by the acid percolates within unsaturated zone of sandstones. *Environ. Monit. Assess.* 185, 7115–7131. <https://doi.org/10.1007/s10661-013-3088-4>.
- Otofujii, Y., Itaya, T., Matsuda, T., 1991. Rapid rotation of Southwest Japan - paleomagnetism and K-Ar ages of Miocene volcanic-rocks of Southwest Japan. *Geophys. J. Int.* 105, 397–405. <https://doi.org/10.1111/j.1365-246X.1991.tb06721.x>.
- Prebble, M.M., 1967. Cavernous weathering in the Taylor Dry Valley, Victoria Land, Antarctica. *Nature* 216, 1194–1195. <https://doi.org/10.1038/2161194a0>.
- Roqué, C., Zarroca, M., Linares, R., 2013. Subsurface initiation of tafoni in granite terrains – geophysical evidence from NE Spain: geomorphological implications. *Geomorphology* 196, 94–105. <https://doi.org/10.1016/j.geomorph.2012.06.015>.
- Rothrock, E.P., 1925. On the force of crystallization of calcite. *J. Geol.* 33, 80–83. <https://www.jstor.org/stable/30059172>.
- Saidov, T.A., Pe, L.L., Kopinga, K., 2015. Crystallization pressure of sodium sulfate heptahydrate. *Cryst. Growth Des.* 15, 2087–2093. <https://doi.org/10.1021/cg501537h>.
- Sampei, Y., Matsumoto, E., Kamei, T., Tokoku, T., 1997. Sulfur and organic carbon relationship in sediments from coastal brackish lakes in the Shimane peninsula district, Southwest Japan. *Geochem. J.* 31, 245–262. <https://doi.org/10.2343/geochemj.31.245>.
- Sancho, C., Benito, G., 1990. Factors controlling tafoni weathering in the Ebro Basin (NE Spain). *Zeitschrift für Geomorphol.* 34, 165–177. <http://pascal-francis.inist.fr/vibad/index.php?action=getRecordDetail&idt=6535833>.
- Schnepfleitner, H., Sass, O., Fruhmans, S., Viles, H., Goudie, A., 2016. A multi-method investigation of temperature, moisture and salt dynamics in tafoni (Tafroute, Morocco). *Earth Surf. Process. Landf.* 41, 473–485. <https://doi.org/10.1002/esp.3838>.
- Schweigitilová, J., Příklad, R., Novotná, M., 2009. Isotopic composition of salt efflorescence from the sandstone castellated rocks of the Bohemian cretaceous Basin (Czech Republic). *Environ. Geol.* 58, 217–225. <https://doi.org/10.1007/s00254-008-1510-y>.
- Shtober-Zisu, N., Amasha, H., Frumkin, A., 2017. Inland notches: lithological characteristics and climatic implications of subaerial cavernous landforms in Israel. *Earth Surf. Process. Landf.* 42, 1820–1832. <https://doi.org/10.1002/esp.4135>.
- Strini, A., Guglielmin, M., Hall, K., 2008. Tafoni development in a cryotic environment: an example from Northern Victoria Land, Antarctica. *Earth Surf. Process. Landf.* 33, 1502–1519. <https://doi.org/10.1002/esp.1620> (in Japanese with English abstract).
- Sunamura, T., 1992. *Geomorphology of Rocky Coasts*. John Wiley & Sons, Chichester.
- Tesoriero, A.J., Pankow, J.F., 1996. Solid solution partitioning of Sr²⁺, Ba²⁺, and Cd²⁺ to calcite. *Geochim. Cosmochim. Acta* 60, 1053–1063. [https://doi.org/10.1016/0016-7037\(95\)00449-1](https://doi.org/10.1016/0016-7037(95)00449-1).
- Turkington, A.V., 1998. Cavernous weathering in sandstone: lessons to be learned from natural exposure. *Q. J. Eng. Geol. Hydrogeol.* 31, 375–383. <https://doi.org/10.1144/GSL.QJEG.1998.031.P4.11>.
- Turkington, A.V., Paradise, T.R., 2005. Sandstone weathering: a century of research and innovation. *Geomorphology* 67, 229–253. <https://doi.org/10.1016/j.geomorph.2004.09.028>.
- Van Kranendonk, M.J., 2006. Volcanic degassing, hydrothermal circulation and the flourishing of early life on Earth: a review of the evidence from c. 3490–3240 Ma rocks of the Pilbara Supergroup, Pilbara Craton Western Australia. *Earth-Sci. Rev.* 74, 197–240. <https://doi.org/10.1016/j.earscirev.2005.09.005>.
- Viles, H.A., Goudie, A.S., 2004. Biofilms and case hardening on sandstones from Al-Quwaira, Jordan. *Earth Surf. Process. Landf.* 29, 1473–1485. <https://doi.org/10.1002/esp.1134>.
- Wasylenki, L.E., Dove, P.M., Wilson, D.S., De Yoreo, J.J., 2005. Nanoscale effects of strontium on calcite growth: an in situ AFM study in the absence of vital effects. *Geochim. Cosmochim. Acta* 69, 3017–3027. <https://doi.org/10.1016/j.gca.2004.12.019>.
- Yoshida, T., 1979. Fluid inclusion study and ore forming process of the Iwami deposit, Shimane prefecture, Japan. *Min. Geol.* 29, 21–31 (in Japanese with English abstract).
- Young, R.G., 1964. Fracturing of sandstone cobbles in caliche-cemented terrace gravels. *J. Sediment. Petrol.* 34, 886–889. <https://doi.org/10.1306/74D711D1-2B21-11D7-8648000102C1865D>.